مدينة الملك عبدالعزيز
للعلوم والتقنية
الإدارة العامة لمنح البحوث

رقم المشروع : أت - 33-14

التقرير النهائي المنقح

التطور الجيوكيميائي والجيوفيزيائي لإنسياب الوشاح الإقليمي تحت الحرات البركانية في غرب الدرع العربي

الفريق البحثي:

د. عبدالله محمد العمري (الباحث الرئيسي)
د. فوزان علي الفوزان (الباحث المشارك)

جامعة الملك سعود

8 محرم 1438 هـ

King Abdulaziz City for Science and Technology
General Directorate of Research Grants Programs

Project No. : AR-33-14

Revised Final Report

Geochemical and Geophysical Evolution of Regional Mantle Flow Beneath Volcanic Harrats in Western Arabian Shield

Reserch team:

Prof. Abdullah M. Alamri (PI)
Dr. Fouzan A. Alfouzan (CO-I)

King Saud University

October 9, 2016

ACKNOWLEDGMENTS

This is the revised final progress report of the research project **AR-33 - 14**. The authors would like to express their thanks and gratitude to King Abdulaziz City for Science and Technology for funding this project. This work would not have been possible without the generous assistance of **KACST**.

Dr. Robert Duncan, the project consultant, whose expert guidance and continuing advice made this work possible. His willingness to devote his time greatly facilitated the completion of the project we owe him a deep debt of gratitude and a great deal of thanks. Grateful acknowledgment is also extended to the anonymous referees for their helpful suggestions and criticism of previous progress reports.

Finally and most importantly, we would like to extend our sincerest thanks to Adam Kent, David Graham, Saeed Al-Shaltoni, Musaed Alharbi and Suhail Alhiji who helped in performing samples collection, age-dating determination as well as processing of geochemical samples.

Table of Contents

List of Tables

List of Figures

List of Abbreviations قائمة الاختصارات

K-Ar : Potassium – Argon

XRF : X-ray fluorescence

R_A : Atmospheric He-isotopic ratio

MMN : Makkah – Madinah – Nafud lineament

LAB : Lithosphere-Asthenosphere Boundary

VLBI : Very-Long-Baseline Interferometry

GPS : Global Positioning System

REE : Rare Earth Elements

الملخص العربي

هذا هو التقرير النهائي للمشروع البحثي التطبيقي أت - 33-14 بعنوان " التطور الجيوكيمائي والجيوفيزيائي لأنسياب االوشاح الاقليمي تحت الحرات البركانية في غرب الدرع العربي" المدعم من مدينة الملك عبدالعزيز للعلوم والتقنية.

نقدم في هذا التقرير النهائي تفصيلا كاملا عن النتائج النهائية للدراسة من ناحية أصل وتطور المناطق البركانية في غرب المملكة العربية السعودية. وتبين أن هذه المتكونات البركانية (الحرات) تولدت من خلال تمدد القشرة الأرضية عبر الدرع العربي، وخصوصا في ما يتعلق من اتساع قاع البحر الأحمر بين الصفيحتين العربية والأفريقية، منذ حوالي 30 مليون سنه. ومع ذلك فإن توزيع البراكين (يتضح في الاغلب في الصفيحه العربية، وتصل إلى تقريبا 500 كيلومتر الى الشرق من حدود الصفيحة العربية من البحر الاحمر)، وتمددها بشكل ملحوظ وواضح ولكن ليس ليس اكثر من ما ذكر تقريبا، ويلاحظ ايضا وجود تغير بين حدود عمق الغلاف الصخري - والغلاف المائع، أدى إلى تكهفات بتداخل منطقة الوشاح في عفار او من تكونات عفار (الموجود ضمن تقاطع الثلاثي الاثيوبي) أو ممكن من أي مكان آخر.

في هذه الدراسة قدمنا نتائج لبيانات جديدة تسمح للباحثين في تقييد العمليات الجيوديناميكية التي تؤدي إلى ميكانيكية الحرات. النقطة الاساسية التي قدمناها ونعالجها في هذه الدراسة هي الاهتمام في الاسباب الاساسية للذوبان او الانصهار ، وخصوصا : (ا) دور الغلاف المائع مقابل الغلاف الصخري في إنتاج صهارة الحرات. (ب) التغييرات المنهجية في عمق وتمدد الذوبان والانصهار في ناحية المكان والزمان، وايضا العلاقة بين الذوبان او الانصهار والتركيب الحراري للوشاح، (ت) واخيرا الدور المحتمل لمواد الوشاح في نشاط براكين الحرات.

جمعنا العديد من الدراسات السابقة ذات الصله بدراستنا، قمنا بالفحص والتحقق من العديد من البيانات السيزمية، وكذلك دراسة الخرائط الجيولوجية، وقمنا ايضا بأخذ ودراسة العديد من العينات الصخرية وتحديد العمر الزمني لها. حققنا بالتالي من خلال هذه الاشياء المهام التالية:

- مراجعة الخرائط والبيانات الجيولوجية السابقة للمنطقة البركانية حرة خيبر الكبيرة، وتشمل ايضا حرات كرا وخيبر وإثنان.
- واستندت العمليات الميدانية في مدينة خيبر، والتي أجرينا عليها دراسة شامله للخرائط الجيولوجية ومنها جمعنا العينات الصخرية. قمنا ايضا بتقييم مدى ملاءمة وصلاحيتها للعمل التحليلي في المستقبل (بتحديد العمر الزمني، وتحديد التراكيب والعناصر الرئيسية).
- قمنا بتحليل جميع البيانات السيزمية الموجوده للمنطقة والتي تم الحصول عليها من المساحه الجيولوجية السعودية وايضا من خلال محطات رصد الزلازل المؤقتة التي تم تركيبها في هذا المشروع.
- أجرينا (1) فحص عديد من العينات الرقيقة جدا للفحص الصخري لعدد 36 عينة وتم عملها في هذا المشروع، (2) اخترنا عينات لعمل فحص وتحديد العمر الزمني بواسطة Ar^{39}-Ar^{40} وهي من خلال طريقة التسخين التدريجي وايضا طريقة النظائر بالاضافة الى دراسة ذوابان والانصهار التداخلي للعينات، (3) حللنا ايضا مكونات التراكيب الاساسية والعناصر للعينات من خلال قياسات الأشعة السينية وتحليل MS-ICP.
- حصلنا على Ar^{39}-Ar^{40} من تحديد العمر الزمني للتركيب الحراري التراكمي، وتركيزات العناصر والتراكيب الأساسية فيها، وتحديد النظائر من تدفقات الحمم من الحرات البركانية المحدد، لكي يتم فهم أفضل للتوزيع الزمني للنشاط بركاني، وايضا تاثيرات مصادر الوشاح المميزة، وتحديد تغيرات العمق ودرجة الذوبان والانصهار لهذه المنطقة. وهناك برنامج الجيوفيزياء تكميلي لمراقبة النشاط الزلزالي في المنطقة، وإنتاج

صور من القشرة الأرضية وبنية الوشاح العلوي تحت العديد من المناطق. وقد ركزنا تحقيقاتنا واستكشافاتنا على المقطع ما بين الشرق والغرب (في ~ 25 درجة شمالا) عبر النطاق شمال - جنوب من هذه المنطقة الكبيرة، بما في ذلك الحقول البركانية الاصغر من حرة هتيمة ولونير ، وايضا للحره الاكبر والاقدم حرة خيبر.

- أجرينا أيضا دراسة بتقنية تحديد الضوضاء للمنطقة باستخدام بيانات اثنا عشر محطة رصد الزلازل من هيئة المساحة الجيولوجية السعودية، وكذلك من محطات رصد الزلازل المتنقله التي انشئت في هذا المشروع. وركزت النتائج المقدمة هنا على الضوضاء المحيطة في داخل المملكة العربية السعودية وخصوصا في الجزء الجنوبي الغربي من حرة خيبر.

وبسبب ان عدد الزلازل التي تم رصدها اغلبها كان صغير وكانت التسجيلات الزلزالية غير شاملة ايضا للمسارات المحدده، وكان التصوير التقليدي للمقاطع الزلزالية باستخدام بيانات الزلازل الموجوده والمرصودة غير كافي لرسم صور عالية الدقة للقشرة العليا حيث من المتوقع وجود غرف الصهارة صغيرة أو الصدوع. وللتغلب على هذه المشكلة، وتقنية تصوير المقطعي الزلزالي لتحديد الضوضاء المحيطة تم استخدامها رسم خريطة صور عالية الدقة من القشرة العليا تحت حرة خيبر .

وقد تم تطبيق هذه التقنية على مختلف المستويات: العالمية والإقليمية والمحلية باستخدام قياسات وسجلات للضوضاء الزلزالي المستمر بدء من بضع ساعات فقط الى تسجيلات لبضعة أشهر. وتستخدم هذه التقنية لاسترداد معادلة قرين **(Green)** من خلال عدد مزدوج من التسجيلات الزلزالية وذلك بتطبيق تقنية تقاطع بين جهازين رصد زلزالي لتسجيلات الضوضاء المحيطة في المنطقة. وهذا اعطى إشارة مكافاءه لتلك التي لوحظت في محطة تسجيل واحده وذلك نظرا لان منطقة سطح المصدر تتفاعل كما انه من مصدر محطة رصد زلزاليه اخرى.

وان الاشارة المرصوده من تقنية التقاطع للاختلاف السعة الطيفية عرضت من خلال الجمع بين تاثير الطيفي لحركة الارض ومعادلة التاثير لمعادلة قرين **(Green)**.

النماذج الجيوديناميكية تصنف إلى فئتين: فعال ذاتي وغير فعال. ومنذ ما يقرب من 30 مليون سنة ماضية، تم انفصال الصفيحة العربية عن الصفيحة الأفريقية على طول امتداد البحر الأحمر وخليج عدن. تم تكون قاع جديد للبحر من خلال الموجات المتقلبة والضغط لذوبان الوشاح العلوي تحت هذه المواقع. وان تمدد القشرة الأرضية يمكن أن يؤثر على هامش حدود هذه الصفائح الجديدة، لينتج التصدعات للقشرة الأرضية. كلتا العمليتين تقلل من المسافة بين حدي الصفيحيتن المنفصلتين. وهكذا يمكن لمناطق الحرات البركانية ان ينتج ردة فعل ذاتيه من خلال تصدع القشرة الأرضية وتقليل سمك الصفيحه عند الاطراف. مع ذلك نحن نتوقع أن النشاط البركاني سوف يكون موزع بشكل متماثل بين جانبي البحر الأحمر، وأن كثافة النشاط البركاني سوف تقل كلما ابتعدنا عن حدود الصفائح، وأن النشاط البركانية يمكن يتاثر كثيرا من ناحية توزيع الصدوع الموجوده والموازية للبحر الاحمر والتي هي باتجاه شمال شرق- جنوب غرب ولكن اي من هذه الاشياء لم تمت ملاحظته هنا. وكما هو معلوم فان توزيع النشاطات البركانية يتمدد تقريبا بحدود 500 كيلو متر على الصفيحة العربية من اطراف البحر الاحمر (ولكن في اغلبها غير ظاهره في جانب الصفيحة الافريقية)، أكبر هذه الحرات البركانية (خيبر، رهط) وتقع بعيده عن البحر الاحمر، واغلب تركيبها الرئيسي مكون من نفوذ مكة المكرمة - المدينة المنورة MMN وهي باتجاه تكوني شمال –جنوب موازي للبحر الأحمر.

وفي العموم فان نماذج الجيوديناميكية النشطة وتشمل تدفق الوشاح العلوي في المنطقة سواء يكون من الأسفل أو أفقيا، وذلك لتوفير المواد الساخنة للذوبان، او ترقق القشرة الأرضية بفعل التعرية الحرارية وتحركها بالرفع بسبب الطفو لهذه المواد. في الاغلب فاذن التدفق الرأسي يكون من خلال الممار الصغير في الوشاح وهي تحت اكبر هذه المواقع البركانية النشطة. التدفق الذي يحصل شمالا ممكن ان يكون بسبب منطقة عفار، وتعرف بي التحرك في الوشاح تكون

تقريبا قبل 32 مليون سنه. وتاكيد هذه النظريات والتكوينات اثبتت من خلال الرصد والدراسات الزلزالية. كما ان نتائجنا في هذه الدراسة تاكد وتثبت هذه النماذج الجيوديناميكية النشطة من خلال:

1. تم توثيق تطور العمر الزمني للنشاط البركاني الموجوده منذ القدم في منطقة خيبر من 8.4 مليون سنه حتى الآن. وتشير المتكونات للحمم انها تبدا تقريبا بالصهار من عمق (60-80 كم) ، ثم بدات تدريجيا بالذوبان من مناطق ضحله بعمق (36 كم) مع مرور الوقت. وهذا يتفق من ان أقل درجة من ذوبان والانصهار واعلى درجة مع ترقق في القشرة الأرضية. فكل هذه التفاصيل تتفق تاريخ مع التفاعل الحراري في الغلاف الصخري
2. تركيب النظائر في بعض الحرات مثل خيبر ورهط اعطى قيم (مع القيم> RA 10) والتي تشير إلى تسببها من مواد متكوانت الوشاح. ولم نتمكن من تمييز التدفق الذي حصل مباشرة تحت هذه الحرات والتي حصل لها التدفق بشكل جانبي من الشمال من منطقة عفار. بالتاكيد فان مزيد من الدراسة للانشطه البركانية في الجنوب من منطقة عملنا سوف تساعد في حل والاجابه على هذه الاستفسارات.
3. أظهر نتائج نمذجة الرصد الزلزالي انخفاض سرعة موجة القص الزلزالية في حدود من 2.0-3.2 كم / ث. واتضحت ايضا ان الجهة الغربية لمنطقة الدراسة شملت اقل سرعة لهذ الموجات. ومن الجدير ذكر ايضا أن منطقة الدراسة تقع الى الشمال الشرقي لمنطقة مركز زلزال الذي وقع في 19 مايو 2009 (ML = 5.4) حيث ان هذه المنطقة يفترض ان يحصل فيها الاختراقات المنصهرة. القشرة المحيطة والتدخل السريع يكون فيها ابطئ من التي اوضحتها نماذج القياس في الدرع العربي. أكبر الأحداث التي وقعت في زمن مبكر كانت قوية وتتراح على اعماق ضحله ما بين 2 – 8 كم خصوصا في

تحت منطقة الشمال من حرة لونير، وكل هذه الاحداث ترتبط بشكل مباشر مع الصدوع والقواطع الموجوده في المنطقة.

من الناحية الجيولوجية، قد تكون هذه الحرات تحوي طاقات حرارية ارضية عاليه تكون ما بين 150 و 300 درجة مئوية ، وبالتالي تكمن أهميتها في انها تكون مصدر مهم ومتجدد للانتاج الطاقة. النتائج المستخلصه من هذه الدراسة تشير الى احتماليه وجود مواد منصهرة بسبب انخفاض سرعة الموجات تحت حرة خيبر نتيجة وجود الصهارة في هذه المنطقة.

Summary

This is the revised final report of the project **AR-33 - 14** entitled " Geochemical and Geophysical Evolution of Regional Mantle Flow Beneath Volcanic Harrats in Western Arabian Shield " sponsored by King Abdulaziz City for Science & Technology (KACST). We conducted three field programs to determine the distribution and structure of volcanic landforms (lava flows, cinder cones, eruptive centers), and to collect samples for analytical studies (age determinations, mineral and whole compositions, isotope geochemistry). The first expedition was to Harrat Lunayyir, where recent seismic activity indicated the possibility of new volcanic systems. The second focused on Harrat Hutaymah, which is remarkable in providing an extraordinary range of mantle and crustal xenoliths, which are fragments of rock carried up from great depths (40-70 km) by magmas that fed lava flows and cinder cones.

In order to achieve the above mentioned tasks:

- We reviewed previous mapping and geologic data for the large Harrat Khaybar volcanic area, comprising Kura, Khaybar and Ithnayn volcanic fields.
- The field operations were based at Khaybar city, from which we conducted mapping and sample collecting. We assessed the suitability for future analytical work (age determinations, major and trace element compositions)**.**
- Analyzed all existing seismic data provided by SGS and temporary seismic stations.
- We performed (1) thin section preparation for petrographic examination of 36 samples, (2) selected samples for age determinations by ^{40}Ar-^{39}Ar incremental heating method and for He isotope and melt inclusion studies, and (3)

analyzed major and trace element compositions by X-ray fluorescence and ICP-MS analysis.

- We acquired new ^{40}Ar-^{39}Ar incremental heating age determinations, major and trace element concentrations, and He-isotopic compositions of lava flows from selected harrats to better understand the temporal distribution of the volcanism, contribution of distinct mantle sources, and variable depth and degree of melting over the region.
- We also performed ambient noise tomography technique using data from twelve seismic stations of the Saudi Geological Survey as well as from deployed portable seismic stations. The results presented here are focused on ambient noise propagating within Saudi Arabia and in the southwestern part of Harrat Khaybar.
- We conclude that Hutaymah and Lunayyir lavas were generated at depths of 60-80 km and small degrees of melting (1-10%), while Khaybar and Rahat lavas were generated under a progressively thinning lithosphere (60-36 km) and increasing extents of melting.
- Lithosphere that is derived from melting of the upper mantle also has this small range of isotopic compositions. In contrast, primitive mantle, which lies below the depleted upper mantle and is delivered to the earth's surface by mantle plumes only at hotspots, exhibits He-isotopic compositions >10 R_A. Lavas and xenolithic fragments from Hutaymah showed that all volcanic and source materials are derived from depleted asthenosphere and lithosphere. Our new data from Khaybar show that initial lavas (6-8 Ma age) have significantly higher He-isotopic compositions (12-13 R_A), while younger lava compositions

are within the range of asthenospheric values. Higher values have also been reported for Harrat Rahat.

- We have produced new data that allow us to constrain the geodynamic processes that lead to harrat magmatism. The key issues we address in this research concern the ultimate causes of melting, specifically: (i) the role of asthenosphere vs. lithosphere in the production of harrat magmas; (ii) systematic changes in the depth and extent of melting in space and time, and the relation between melting and mantle thermal structure, and (iii) the potential role of mantle plume material in harrat volcanism.
- Seismic tomographic inversion shows low shear wave velocity in the range of 2.0-3.2 km/s. The study area is clearly resolved with the lowest group velocity toward the west. It is worthy to mention that the study area is located toward the northeast of the epicenter of the 19th of May 2009 (ML = 5.4) where the area is presumably enriched with magmatic intrusions.

Introduction

We report the final results of a study of the origin and evolution of volcanic fields in western Saudi Arabia. These volcanic systems (harrats) appear to reflect lithospheric extension across the Arabian shield, related to Red Sea opening between the Arabian and African plates, since about 30 Ma. However, the distribution of the volcanism (predominantly Arabian plate, and up to 500 km east of the plate boundary), lack of significant extension, and variable depth of the lithosphere - asthenosphere boundary, have led to speculation of mantle plume involvement either from the Afar plume (located under the Ethiopian triple junction) or from elsewhere.

Firstly, we have acquired new ^{40}Ar-^{39}Ar incremental heating age determinations, major and trace element concentrations, and He-isotopic compositions of lava flows from selected harrats to better understand the temporal distribution of the volcanism, contribution of distinct mantle sources, and variable depth and degree of melting over the region. In a complementary geophysics program we monitored seismic activity, and produced images of crustal and upper mantle structure beneath several of the fields. We have focused our investigations on an east-west transect (at ~25°N) across the predominant N-S fabric of the province, including the smaller volcanic fields of Harrat Hutaymah and Lunayyir, and the large and long-lived Harrat Khaybar (Figure 1).

Secondly, we performed ambient noise tomography technique using data from twelve seismic stations of the Saudi Geological Survey and from seismic portable stations as well. The results presented here focus on ambient noise propagating within Saudi Arabia and in the southwestern part of Harrat Khaybar (Figure 2).

Due to the small number of earthquakes and the lack of travel paths covered by seismograms, the traditional seismic tomography using earthquake data is not adequate to map high resolution images of the upper crust where small magma chambers or dykes are expected. To overcome this problem, the ambient seismic-noise tomography technique can be used to map high resolution images of the upper crust beneath Harrat Khyabar (Shapiro et al., 2005). This technique has been applied on different scales; global, regional and local using only a few hours to a few months of continuous records of seismic noise (Bensen et al., 2007). This technique is used to retrieve the Green's function between pairs of seismograms by applying the cross-correlation technique on the ambient noise recorded at two seismic stations. This gives an equivalent signal to that observed at one recorded station due to a surface point-source acting at the location of the other station. The retrieval signal from cross-correlation technique exhibited spectral amplitudes combined the effects of the ambient ground motion spectra and the Green's function excitation.

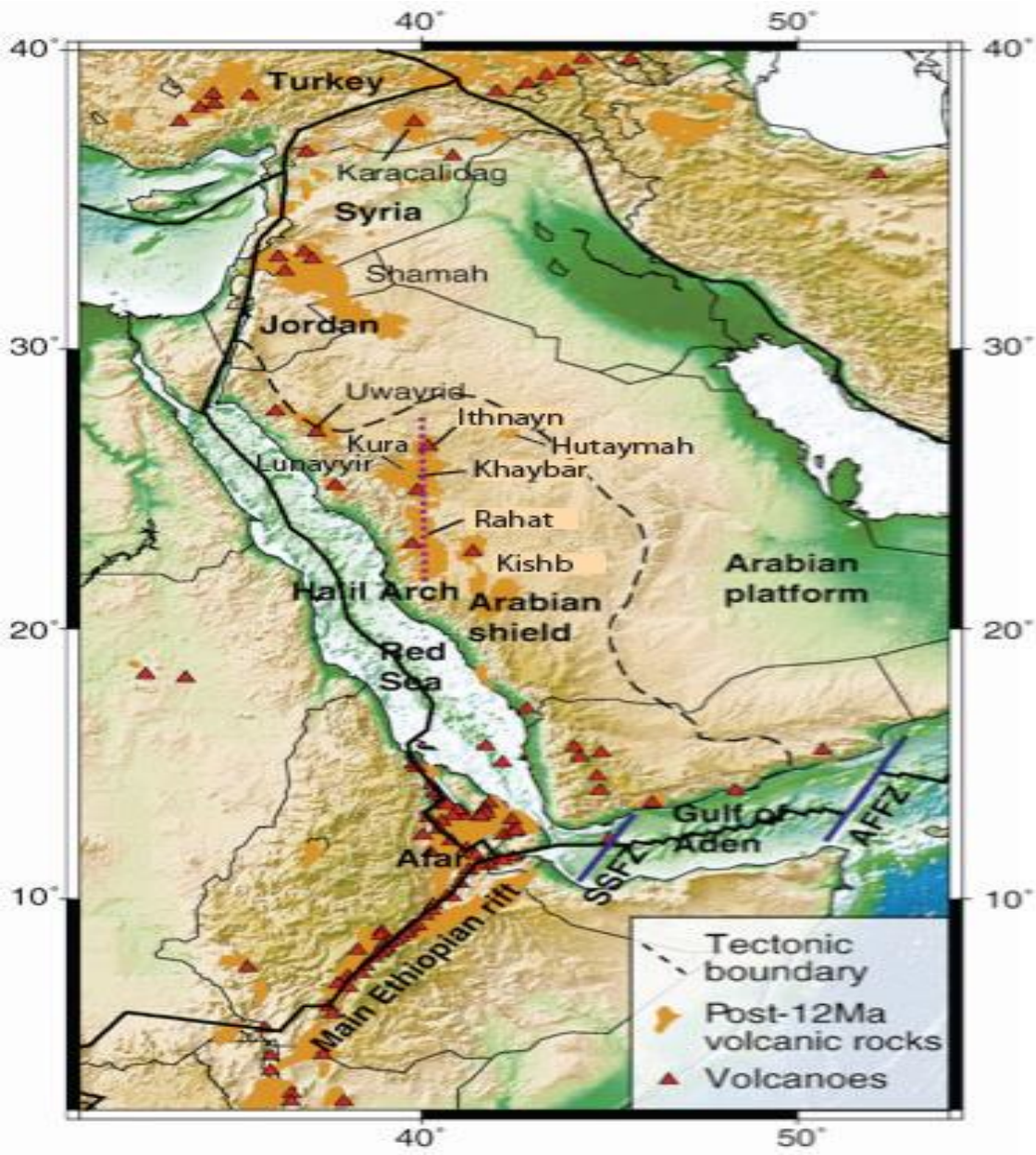

Figure 1. Volcanic fields ('harrats') in western Saudi Arabia lie 100-500 km east of the Red Sea spreading ridge, and are linked to similar accumulations of lava flows in Yemen and the Afar region in Ethiopia/Eritrea to the south, and Jordan, Syria and Turkey to the north (Figure adapted from Chang and van der Lee, 2011). Several large volcanic fields are aligned with the Ha'il Arch structure and form the north-south trending Makkah-Madinah-Nafud lineament.

26.11º N

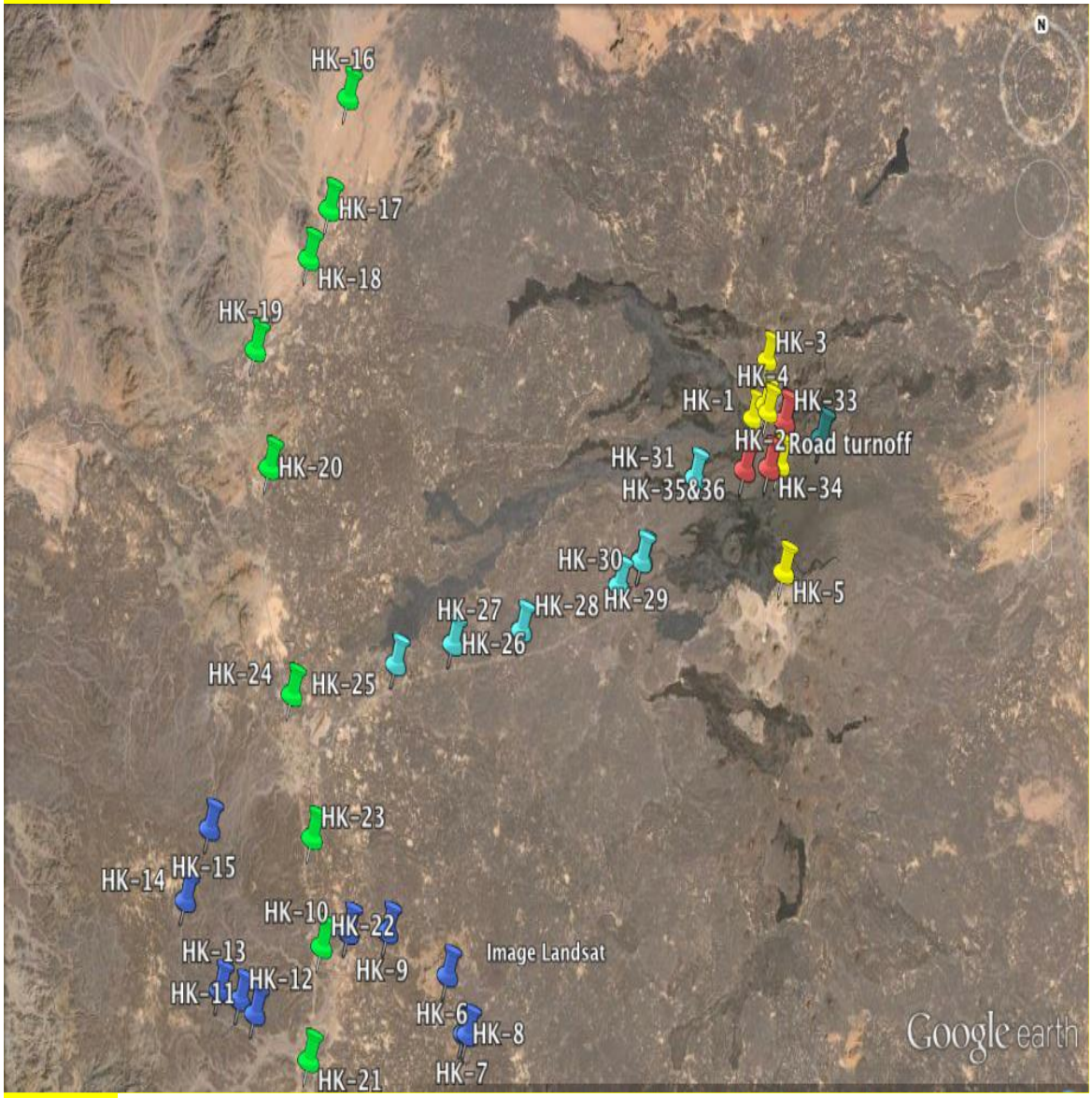

25.28º N

39.35º E **39.55º E** **39.96ºE**

Figure 2. Google Earth™ image of Harrat Khaybar showing 2014 sample locations. Youngest, possibly historic lava flows are clearly seen as black (unaltered) surfaces. Some of these are known to have flowed over Neolithic sites, confirming their recent age.

Literature Review

The western part of the Arabian Shield is made up of three major accreted tectono-stratigraphic terranes (Asir, Jeddah and Hijaz) consisting mainly of variously metamorphosed layered volcano-sedimentary assemblages of older Baish, Bahah and Jeddah groups (950-800 Ma) and younger Halaban (Hulayfah) and Al Ays groups (800-650 Ma old: e.g.,) with arc-related plutonic rocks of diorite to tonalite compositions, which generally have intrusive relationship with the volcano-sedimentary sequences (Stoeser and Camp, 1985; Johnson, 2000). The Cenozoic to Recent basaltic lava fields (harrats) of Saudi Arabia are resting directly on the so-called stable Precambrian Arabian Shield. The application of remote sensing to the lava fields of Saudi Arabia has been realized on Harrat Rahat (Camp and Roobol, 1992), Harrats Khaybar, Ithnayn and Kura (Roobol and Camp, 1991a) and Harrat Kishb (Roobol and Camp, 1991b). No such study has yet been made of Harrat Lunayyir and there is no detailed geological map of the lava field.

The existence of a mantle plume beneath the western part of the Arabian plate including Al-Madinah Al-Munawwarah region including Harrat Lunayyir has been recognized (e.g., Moufti and Hashad, 2005). About 600 km long Makkah-Madinah-Nafud (MMN) active volcanic line, consisting of Harrats Rahat, Khaybar, and Ithnayn, is the surface expression of the plume-related ocean-island basalt (OIB) volcanism (e.g., Moufti and Hashad, 2005) and northward propagating nascent rift system (Camp and Roobol, 1992). The last two historic volcanic eruptions, close to the city of Al-Madinah Al-Munawwarah occurred at about 641 A.D. and then again at 1256 A.D.

Two distinct phases of continental magmatism are evident in western Saudi

Arabia. The first, erupted from about 30 to 12 Ma, produced tholeiitic-to-transitional lavas emplaced along NW trends. The second, from about 12 Ma to present, produced transitional-to-strongly-alkalic lavas emplaced along N-S trends. The older phase, predominantly dikes and smaller centers proximal to the Red Sea, is attributed to passive-mantle upwelling during extension of the Red Sea basin, whereas the younger phase is attributed to active-mantle upwelling facilitated by minor continental extension perpendicular to plate collision (Hempton, 1987). The younger magmatic phase is largely contemporaneous with a major period of crustal uplift that produced the west Arabian Swell after about 14 Ma.

Geophysical methods (seismic, magnetics, heat flow) provide images of the crust and upper mantle beneath the western Arabian shield, which must relate closely to the dynamic history of mantle flow, lithospheric uplift, and volcanic activity. Upper mantle flow beneath the region comes from seismic anisotropy studies (Hansen et al., 2006, 2007). Recently, Chang and van der Lee (2011) report jointly inverted teleseismic S- and SKS-arrival times, regional S- and Rayleigh waveform fits, fundamental-mode Rayleigh-wave group velocities, and independent Moho constraints that provide complementary resolution for the three-dimensional (3-D) S-velocity structure beneath East Africa and Arabia. Their tomographic results help reconcile some of the competing explanations for the region's volcanism, uplift, and rifting.

The lava field of Harrat Lunayyir, on the western edge of the central portion of the N-S trend (west of Khaybar), has been selected for high-resolution age, composition and geophysical investigation by Duncan and Al-Amri (2013). This study was initiated because Harrat Lunayyir experienced multiple seismic swarms since 2007. Recent studies (e.g. Pallister et al., 2010) have indicated that these swarms

are associated with magma that has risen to shallow levels beneath Harrat Lunayyir, potentially increasing the likelihood of a volcanic eruption. It is estimated that at least twenty-one different eruptions have occurred in western Arabia over the past 1500 years (Camp et al., 1987), including one near Harrat Lunayyir about 1000 years ago. Some 24 new age determinations by the ^{40}Ar-^{39}Ar incremental heating method detail the volcanic history, which is generally younger than previously thought (Duncan and Al-Amri, 2013). That is, eruptions occurred within the Quaternary period, beginning about 0.6 Ma, and increased in frequency into historic times.

Research Methodology

We have designed three complementary research themes to accomplish the project objectives:

1. **Geochronology**. Samples of previously mapped units in the volcanic stratigraphy of several selected harrats (Lunayyir, Kura, Khaybar, Ithnayn and Hutaymah) were partly dated by the ^{40}Ar-^{39}Ar incremental heating method to determine the time frame of activity. This method is both more accurate and has higher precision than the K-Ar method (by which the previous ages were determined) in its ability to identify and eliminate the effects of ^{40}Ar-loss and mantle-derived ("excess") Ar.

Additionally, new generation multi-collector mass spectrometers have superior sensitivity, lower volume extraction lines, and higher resolution – allowing smaller amounts of radiogenic ^{40}Ar to be resolved; hence younger age limits. Duncan and Al-Amri (2013), for example, show that lavas at Harrat Lunayyir are significantly younger than previously estimated. New ages will be measured at Oregon State University using an ARGUS-VI five-collector mass spectrometer combined with CO2-laser for incremental heating of samples. The 1MW TRIGA research reactor at Oregon State University is used for neutron irradiation of geologic samples, required for this method. New ages were measured at Oregon State University using an MAP 215/50 mass spectrometer equipped with a single ion multiplier operated in peak-hopping mode, and a newly commissioned ARGUS VI five-collector mass spectrometer. Ages are combined with unit volume estimates (from US Geological Survey-Saudi Geological Survey mapping) to obtain eruption rates throughout the volcanic history. Such age data will provide information about frequency of eruptions,

and whether volcanic intensity is building or waning at each center. An important broader impact of this knowledge will be in the evaluation of the geothermal energy potential of several individual harrats (see Utilization of Results below).

2. **Geochemistry**. Major elements (Si, Al, Ca, Mg, Fe, K, Na, Ti, P, Mn) and trace elements (Ni, Cr, Cu, Zr, Ba, Zn, Sr, Nb, Cs, Rb, Th, U, Pb, Ta, Sc, V, Y, REEs) compositions (determined by XRF and ICP-MS methods) will be used to document variability in parental magmas through time and space within the province.

Specifically, samples from an E-W transect of volcanic centers (Hutaymah, Ithnayn, Khaybar, Kura and Lunayyir) are examined for evidence of depth and degree of mantle melting, in order to test the proposed (Camp and Roobol, 1992) used major element compositions to establish pressure and temperature conditions, and degree of melting, using the approach pioneered by McKenzie and Bickle (1988) based on the experimental petrology database. We also used trace element compositions to determine depth and extent of melting (e.g., Zr/Nb, La/Yb), following the strategy of Fram and Lesher (1993). We also evaluated crustal magma chamber processes (e.g., crystal fractionation, crustal assimilation, magma recharge) using major and trace element chemistry as well as analyses of individual mineral phases.

In addition, the melt inclusions in early formed phenocrysts (olivine and pyroxene) and potentially also in mantle xenoliths common in many of the centers (e.g., Hutaymah), were determined using electron microprobe and ICP-MS laser ablation methods to identify the composition of primary melts, formed in the melting zone before homogenization of discrete melts into parental magmas (e.g. Kent et al., 2002; Kent, 2008).

Using the noble gas laboratory at Oregon State University, equipped with a Nu Instruments Noblesse mass spectrometer, we performed isotopic analyses (He, Ne) on

selected samples of ultramafic xenoliths, and olivine-bearing lavas, to distinguish mantle sources for harrat volcanoes. In particular, these data used to evaluate asthenospheric, Afar mantle plume, or sub-continental Arabian shield mantle as potential contributors to melting that produced harrat volcanism.

3. **Geophysics**. We investigated the velocity structure beneath Harrat Lunayyir using seismic travel-time tomography. In this method, absolute and relative travel-times from local and regional earthquakes are inverted for improved event relocations and models of seismic velocity structure. These data will allow us to delineate magmatic features, such as magma pathways, and seismic structures beneath the harrats, thereby giving us considerable information about the three-dimensional structure and modification of the Arabian shield crustal rocks.

Seismic data were collected from all available deployed portable and permanent broadband stations in harrats Lunayyir, Khyber and Rahat. Broadband stations were equipped with either Streckeisen STS-2 or Trillium 120 seismometers while short-period stations equipped with SS-1 Ranger.

We investigated the crustal and upper mantle velocity structure beneath Harrat Lunayyir using body wave travel-time tomography. A number of different earthquake tomography packages are available, such as SIMULPS (Thurber, 1983; Thurber and Eberhart-Phillips, 1990; Hansen et al., 2004) and tomoDD (Zhang and Thurber, 2003; Pesicek et al., 2010), which invert absolute and relative travel-times from local and regional earthquakes for improved event relocations and models of seismic velocity structure. Seismic velocity in a given region depends on the rock characteristics, such as porosity, fracturing, and fluid saturation, and its physical condition, such as temperature and pressure. In volcanic environments, such as Harrat Lunayyir, the presents of fluids, cracks, and gas can also change the elastic properties (Sato et al.,

1989). Hansen et al. (2004) used the travel-time tomography approach to relocate seismic events and determine the velocity structure beneath the south flank of the volcano.

In Harrat Lunayyir, tomographic velocity variations determined with this approach allowed us to differentiate between the slow seismic velocities associated with magmatic features and the fast seismic velocities in the surrounding regions, thereby giving us considerable information about the three-dimensional structure. Additionally, the accurate earthquake locations determined as part of the tomographic analysis helped to delineate the seismic structures in the crust beneath the harrats.

Results & Data Analysis

We conducted three field programs to determine the distribution and structure of volcanic landforms (lava flows, cinder cones, eruptive centers), and to collect samples for analytical studies (age determinations, mineral and whole compositions, isotope geochemistry). The first expedition was to Harrat Lunayyir, where recent seismic activity indicated the possibility of new volcanic systems. The second focused on Harrat Hutaymah, which is remarkable in providing an extraordinary range of mantle and crustal xenoliths (Thornber, 1994), which are fragments of rock carried up from great depths (40-70 km) by magmas that fed lava flows and cinder cones.

In November/December, 2014 we sampled an extensive area of Harrat Khaybar (Figure 2). This volcanic field is constructed from lava flows, tephra and spatter cones that include mainly primitive alkali olivine basalt and basanite compositions. These compositions contrast with the predominantly tholeiitic, fissure-fed basalts found along the eastern margin of the Red Sea (Figure 3).

Hutaymah is constructed from lava flows, tephra and spatter cones that include mainly primitive alkali olivine basalt and basanite compositions (Figure 4). These compositions contrast with the predominantly tholeiitic, fissure-fed basalts found along the eastern margin of the Red Sea. The Hutaymah lava flows were erupted through Proterozoic arc-associated plutonic and meta-sedimentary rocks of the Arabian shield, and commonly contain a range of sub-continental lithospheric xenoliths. Previous radiometric dating of this volcanic field (a single published K-Ar age; 1.8 Ma) is suspiciously old given the field measurement of normal magnetic polarity only (i.e. Brunhes interval, ≤780 ka). Our new age determinations (n=14) are all younger than ~850 Ka, and constrain the time frame of volcanism to 200-850 Ka

(Table 1). Major, trace and rare earth element compositions are compatible with 3-7% upper mantle melting at depths of 60-75 km (Figure 5). We see no significant effect of crustal assimilation in the composition of the lava flows (Figure 6). He-isotopic compositions of xenoliths and lavas are remarkably homogeneous at 7.55 ± 0.03 R_A (2s, n=18) – see Figure 6. Our findings are reported in two manuscripts being prepared for submission (Konrad et al., 2016; Duncan et al., 2016).

Khaybar is a much larger volcanic system, located along the Makkah-Medinah-Nafud lineament above thinner lithosphere. Primitive lava compositions here are similar to those at Hutaymah, but much more evolved compositions (trachytes, phonolites, comendites) also occur, providing evidence of shallow depth (crustal) magma chambers. This harrat has had a much longer record of volcanism) -- mapped as four distinct formations (Kura, Jarad, Mukrash and Abyad) by Camp et al. (1991a) (Figure 7).

Our new ages (e.g., Figure 8) indicate activity at 6.3-5.9 Ma for Kura flows, 1.7-1.5 Ma for Jarad flows, 1.4-0.4 Ma for Mukrash flows, and 0.3 Ma to historic for Abyad flows (Table 2). Thus, we find a significant hiatus (5.9 to 1.7 Ma) within the otherwise continuous volcanic record. Initial measurements of He-isotopic compositions are remarkably homogeneous at 8.2 ± 0.1 R_A (2s, n=3). Major, trace and rare earth element compositions are similar to neighboring (to the south) Harrat Rahat, and indicate that primitive magmas formed from 10-18% partial melting of depleted peridotite at 15-40 km depth. In addition, we see an intriguing trend of increasing degrees of melting at shallowing depths, with time (Zr/Nb and La/Yb trends, Figure 9), which we interpret as evidence for thinning of the lithosphere.

In contrast, magmas at Harrat Lunayyir (100 km east of the Red Sea) formed at 65-80 km depth from 8-12% upper mantle partial melting. Tholeiitic magmas erupted

at the Red Sea spreading axis derive from ~ 25% partial melting of upwelling depleted upper mantle, at depths of 0-10 km. This regional variability in mantle melting can be explained by modest lithospheric extension and mantle decompression melting coupled with northward asthenospheric flow from the Afar hot spot. However, a geochemical contribution to harrat volcanism from Afar plume material is so far missing, or very minor.

Petrographic Description

Sample collection of volcanic rocks from Harrat Khaybar has been archived and stored at the Department of Geology & Geophysics, King Saud University. We selected pieces of the large samples to begin petrographic description and various analytical methods. We had standard petrographic thin sections made for 44 of the samples, from which we have evaluated mineralogy, rock type, and suitability for Ar-dating and geochemical compositions. Our collection contains predominantly primitive alkali basalt and basanite compositions, as well as several more evolved rock types, such as comendite and phonolite. Further refinement of rock classification awaits major element compositions by x-ray fluorescence at Washington State University.

Ar-Dating

All samples appear to be nearly unaltered and suitable for radiometric dating by ^{40}Ar-^{39}Ar incremental heating methods (McDougall and Harrison, 1988). We chose 36 representative samples, spanning all mapped (Camp et al., 1991b) geological formations (Kura, Jarad, Mukrash, Abyad), for initial work. These have all provided excellent, very precise plateau ages from simple age spectra (summarized in Table 2). The oldest formation (Kura basalts) are 8.4-5.9 Ma; Jarad basalts are 1.7-1.5 Ma;

Mukrash basalts are 1.70-0.4 Ma; Abyad basalts are 0.4-presently active. Thus, we can document earliest volcanic activity in this region beginning about 8.4 Ma (late Miocene). There was a significant break in activity, 5.9-1.7 Ma, followed by continuous activity 1.7 Ma to present.

Geochemical Composition

We prepared 36 sub-samples for major and trace elements by x-ray fluorescence, and rare earth elements by inductively-coupled plasma mass spectrometry. These are presently awaiting instrument time for analyses. When these data are available, we will use them to characterize the lava flows, and model mantle melting and crystal fractionation through the 8 m.y. time frame of this volcanic activity. We also selected an initial 22 samples that contain phenocrystic olivine, for He-isotopic analyses. Results from 12 of these samples indicate a narrow range of $^{3}He/^{4}He$ values = 7- 8.3 R_A (where R_A is the atmospheric He-isotopic ratio) for the Jarad. Mukrash and Abyad units; however, several Kura lava flows contain significantly higher values (12-13 R_A). Similar higher values are found at Rahat (Murcia et al., 2015). Our interpretation is that these higher values indicate significant participation of asthenospheric mantle flow from the Afar plume northward beneath the Arabian shield. In addition, we see an intriguing trend of increasing degrees of melting, at shallowing depths, with time (Zr/Nb and La/Yb trends, Figure 9), which we interpret as evidence for thinning of the lithosphere.

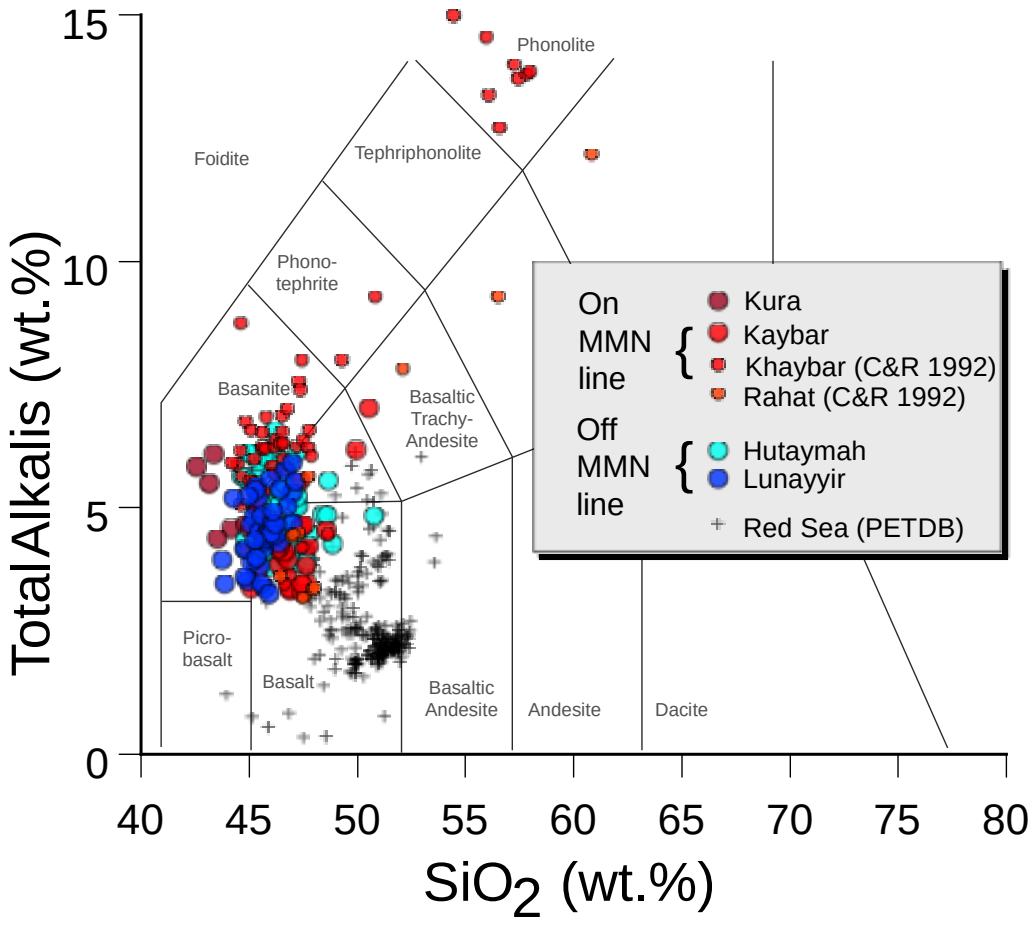

Figure 3. Total alkalis vs. silica. Incudes data from Camp et al. (1991a) and related studies. More evolved compositions occur in harrats from the MMN line, compared with those on the E or W margins of the harrat province.

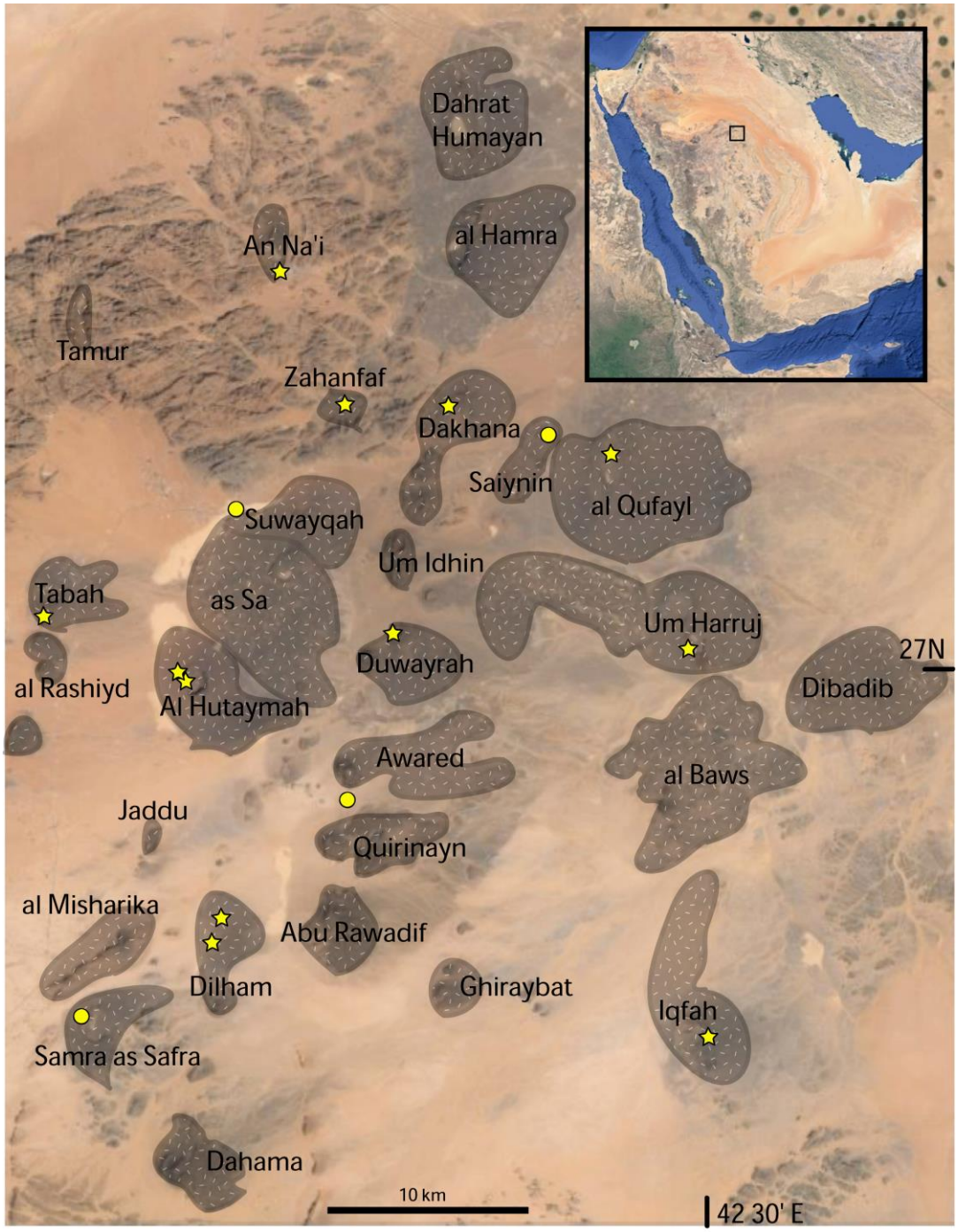

Figure 4. Harrat Hutaymah (location shown in inset) is comprised of lava flows and tephra, sourced from N-S aligned cinder cones, shown with local names. Xenolith localities are yellow stars and circles (from Konrad et al., 2016).

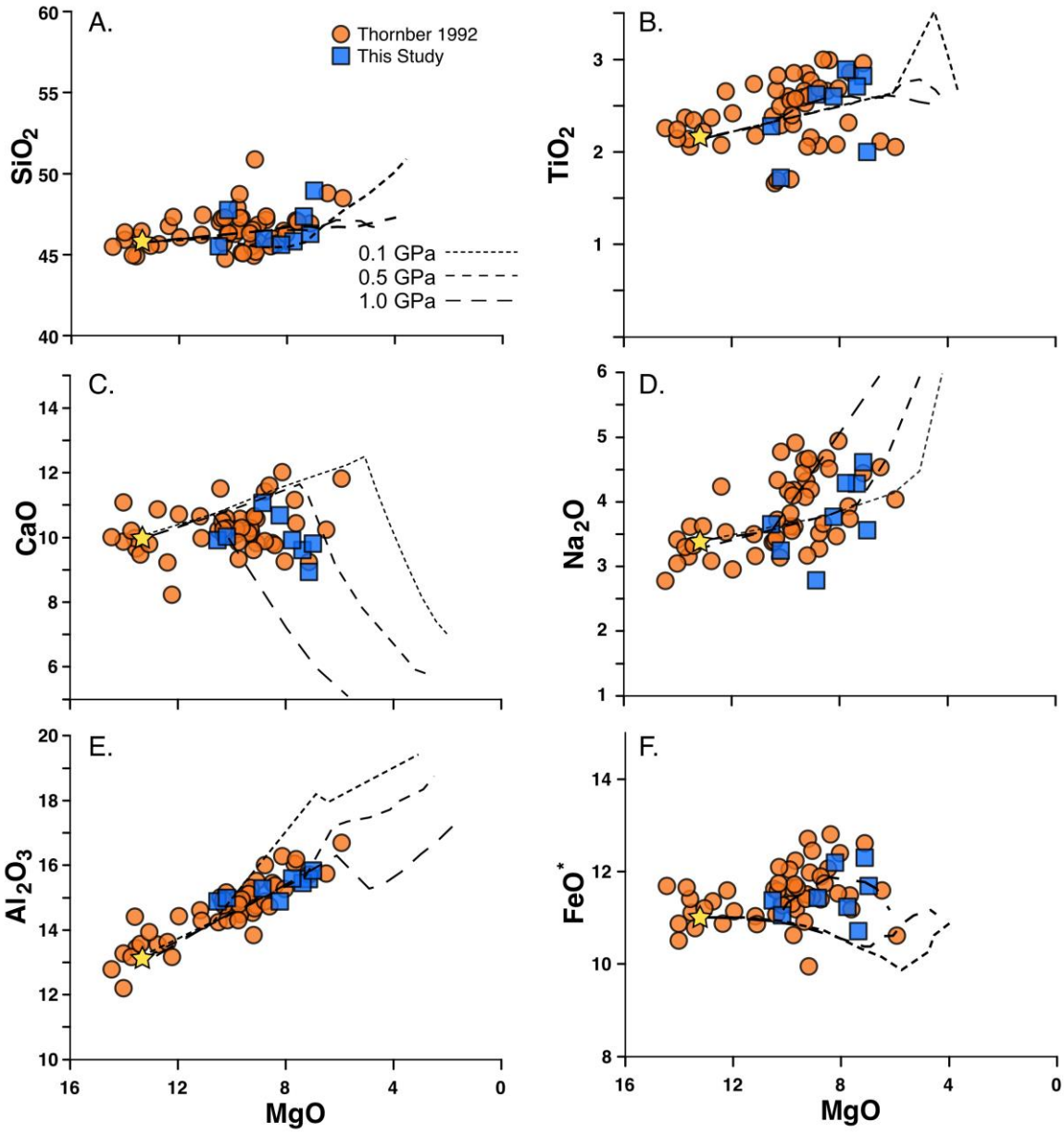

Figure 5. Variations in selected major element oxide vs MgO in Harrat Hutaymah lavas and tephras from Thornber (1992) and this study. Also shown are calculated liquid lines of descent fro fractional crystallization of a representative primary mantle melt (yellow star). Oxidation conditions are at the QFM buffer and 0.2 wt% H2O in the melt.

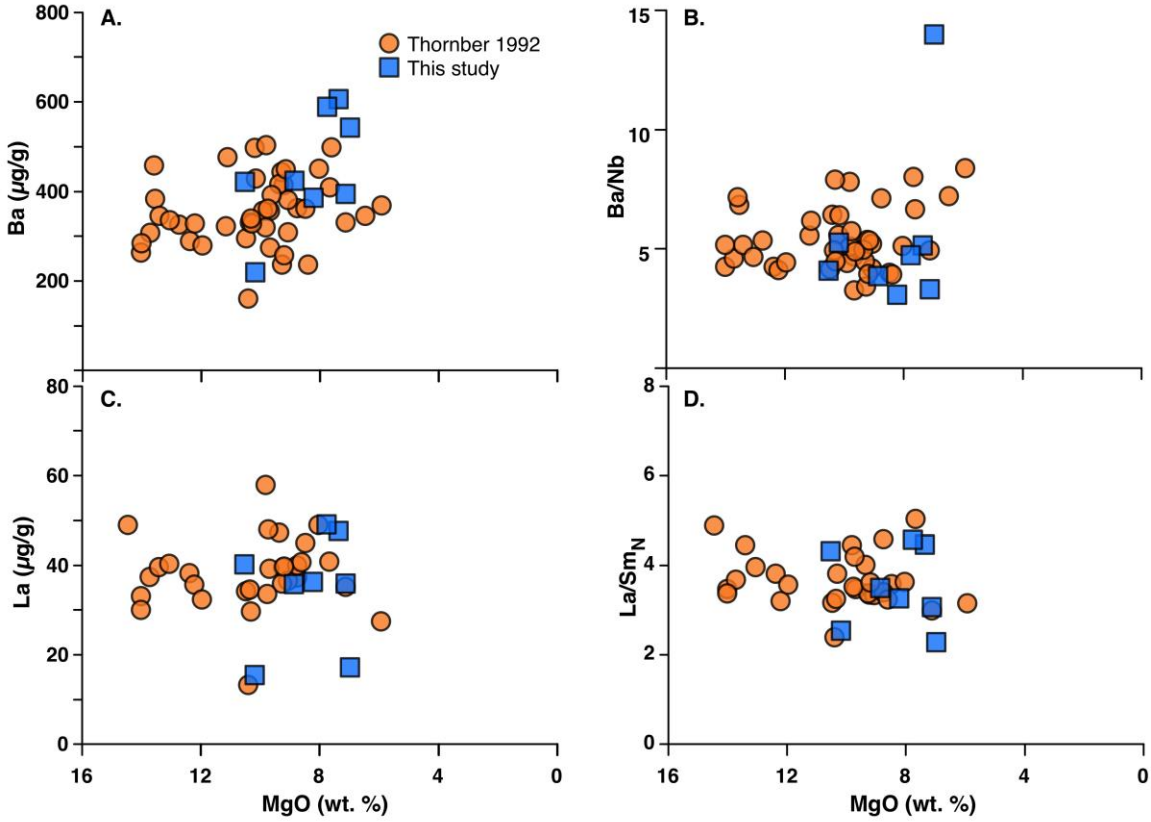

Figure 6. MgO vs (A.) Ba, (B.) Ba/Nb, (C.) La, (D.) La/Sm$_N$. The lack of correlation of these parameters with MgO is evidence that crustal assimilation is minimal.

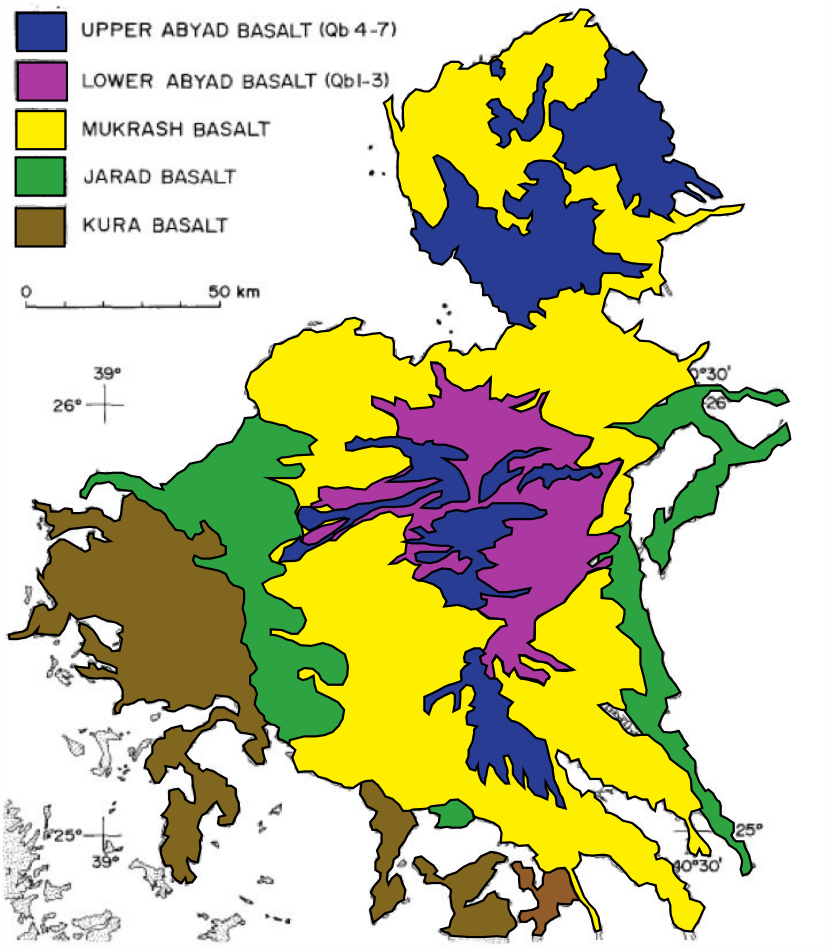

Figure 7. Schematic geologic map of Harrat Khaybar (from Camp et al., 1991a). Volcanic formations are based on stratigraphic position and geomorphologic data. Kura basalt is ~8.3-5.9 Ma; Jarad, Mukrash and Abyad basalt units are 1.7-0 Ma.

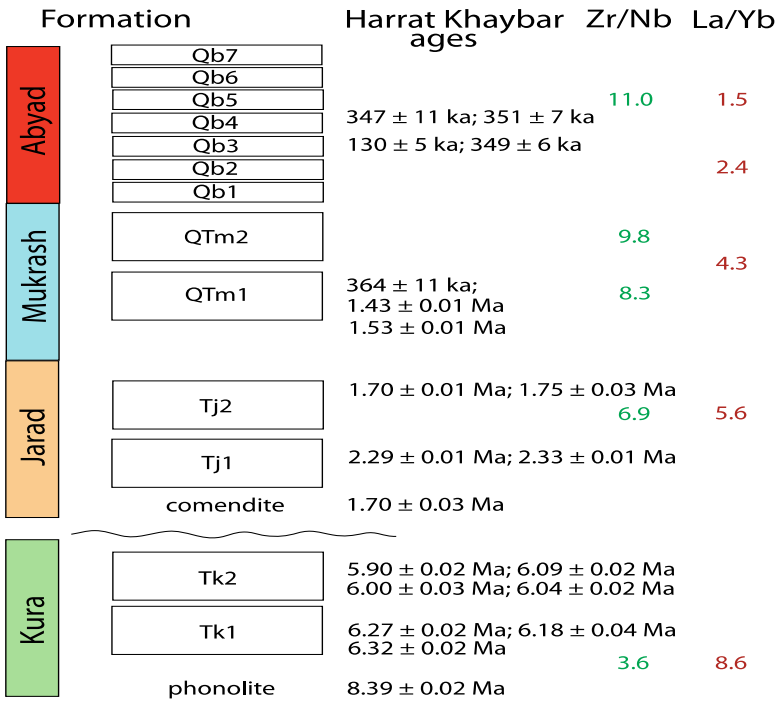

Figure 8. Khaybar stratigraphic section showing mapped formations and units (Camp et al., 1991a), with new plateau ages. Ages conform with stratigraphic position and reveal an unrecognized major hiatus between Jarad and Kura formations of >4 m.y. Trace element ratios indicate degree of mantle melting (Zr/Nb) and depth of last equilibration (La/Yb), using published (Camp et al., 1991a,b) and new data. With time, magmas appear to have been generated by increasing degrees of melting at shallower depths, probably related to thinning of the continental shield beneath this region.

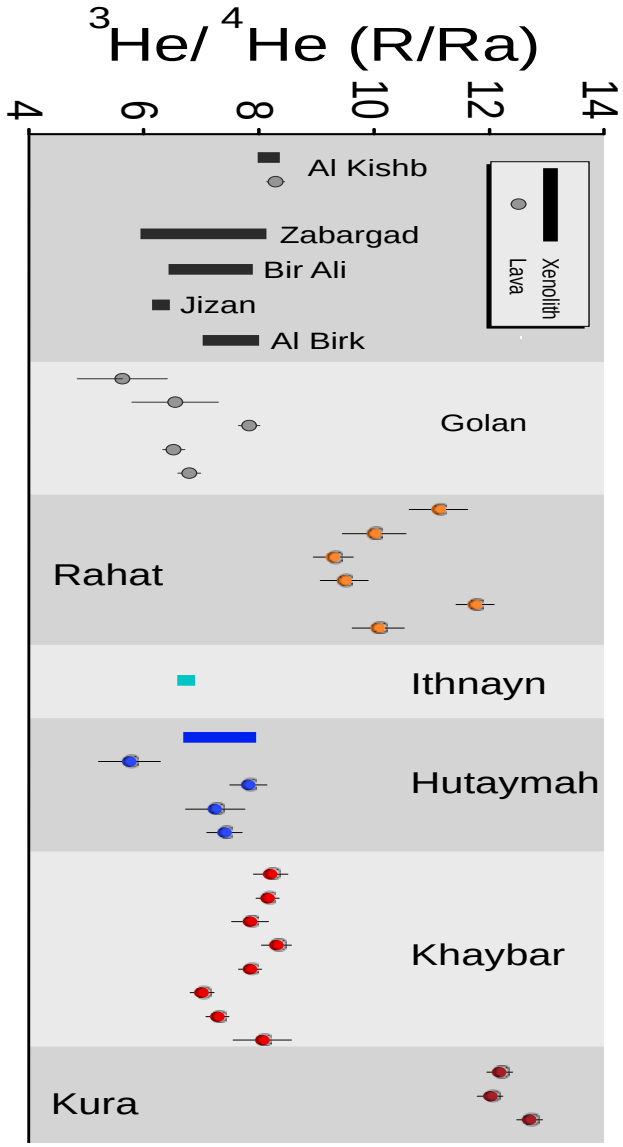

Figure 9. He-isotopic composition in new xenolith and lava flow samples from several harrats and the Red Sea (Zabargad Island). Compositions are remarkably uniform at given volcanic fields, and regionally form a narrow range (6-8 R_A), reflecting primary sub-continental lithosphere and metasomatic fluid resetting since late Proterozoic time (~600-700 Ma). There is evidence for significant participation of asthenospheric mantle flow from the Afar mantle plume in the high values reported from Harrat Rahat (Murcia et al., 2015) and our latest analyses of Kura unit lava flows at Harrat Khaybar (12-13 R_A).

Table 1: 40Ar-39Ar Age Determinations for Lava Flows from Harrat Hutaymah, western Saudi Arabia

Sample	Total Fusion (Ka)	2s error (Ka)	Plateau Age (Ka)	2s error (Ka)	N	MSWD	Isochron Age (Ka)	2s error (Ka)	40Ar/36Ar initial	2s error	Comment
HH-1	246	138	**259**	**120**	16/16	0.51	351	193	295	1	
HH-3	*2340*	*1070*	*not developed*				*not developed*				excess 40Ar
HH-4	*2650*	*580*	*not developed*				*not developed*				excess 40Ar
HH-6	857	474	**729**	**266**	12/16	1.22	1009	525	295	2	
HH-9	471	161	**436**	**97**	14/16	0.69	497	160	295	1	
HH-10	704	48	**709**	**62**	16/16	2.14	712	131	296	3	
HH-11	832	39	**844**	**44**	14/16	1.65	785	115	297	2	
HH-12	581	125	**630**	**82**	33/33	1.30	833	162	294	1	
176688	436	617	**955**	**545**	13/17	0.23	18	1453	298	3	
176691	1140	8	1085	103	19/31	47.10	**818**	**37**	340	5	excess 40Ar
176701a	826	207	**818**	**203**	17/17	0.54	431	290	298	3	
176701b	2339	25	1765	255	31/31	>100	**893**	**44**	331	1	excess 40Ar
176710a	4290	480	*not developed*				*not developed*				excess 40Ar
176710b	980	9	**848**	**8**	14/31	0.43	838	25	302	14	
176712	8040	590	4580	1750	11/17	16.58	**550**	**460**	304	1	excess 40Ar
176734a	930	114	**868**	**90**	16/17	0.46	703	175	298	2	
176734b	881	9	**804**	**10**	19/30	1.54	784	19	307	10	

Ages calculated using sanidine monitor FCs (28.201 Ma) and the total decay constant λ = 5.530E-10/yr. N is the number of heating steps (defining plateau/total); MSWD is an F-statistic that compares the variance within step ages with the variance about the plateau age. Preferred ages are shown in bold; italics indicate sample with suspected mantle-derived (excess) 40Ar.

Table 2: 40Ar-39Ar Incremental Heating Age Determinations for Harrat Khaybar lava flows											
Sample	**Lat. (N)**	**Long. (E)**	**Formation**	**Rock Type**	**Age (Ma)**	**error (±2s)**	**%39Ar**	**MSWD**	**3He/4He**	**[He] cc/g**	Zr/Nb
HK-2	25°48'37.3"	39°56'51.5"	Abyad	alkali basalt	0.347	0.011	69.0	1.11			13.7
HK-3	25°50'25.9"	39°57'10.7"	Abyad	alkali basalt	0.349	0.006	86.6	1.34	8.20 ± 0.30	5.13E-08	10.3
HK-28	25°39'37.3"	39°45'14.4"	Abyad	alkali basalt	0.351	0.007	85.0	0.80			13.4
HK-29	25°40'46.1"	39°47'01.5"	Abyad	alkali basalt	0.128	0.012			8.15 ± 0.20	2.62E-08	8.5
HK-30	25°40'50.3"	39°47'05.4"	Abyad	alkali basalt	0.024	0.006					8.5
HK-31	25°44'42.6"	39°51'18.6"	Abyad	alkali basalt	0.146	0.018			7.85 ± 0.32	3.16E-08	12.6
HK-32	25°46'28.7"	40°01'16.0"	Abyad	alkali basalt	0.130	0.005	76.0	1.28			9.7
HK-33	25°47'19.4"	39°58'24.1"	Abyad	alkali basalt					8.31 ± 0.26	3.29E-08	8.7
HK-34	25°45'05.1"	39°57'08.0"	Abyad	alkali basalt	0.289	0.017					8.0
HK-36	25°45'02.7"	39°55'13.9"	Abyad	alkali basalt	0.560	0.020	54.0	1.40			
HK-5	25°40'04.6"	39°58'08.7"	Mukrash	comendite	1.70	0.03	71.1	1.00			8.2
HK-16	26°03'38.2"	39°24'08.2"	Mukrash	alkali basalt	1.90	0.01		1.68	8.06 ± 0.50	6.44E-10	9.2
HK-19	25°51'25.5"	39°16'39.2"	Mukrash	alkali basalt	1.76	0.02		1.22			10.1
HK-25	25°36'03.5"	39°27'36.2"	Mukrash	alkali basalt	0.449	0.012		1.55	7.01 ± 0.20	1.69E-08	9.9
HK-27	25°37'33.4"	39°37'31.7"	Mukrash	alkali basalt	0.364	0.011	97.2	0.61			10.7
HK-26	25°36'58.3"	39°32'07.1"	Mukrash	alkali basalt	1.43	0.01	74.0	1.52	7.28 ± 0.20	2.37E-08	9.9
HK-6	25°21'04.4"	39°31'29.0"	Jarad	alkali basalt	1.53	0.01	50.2	1.41	7.85 ± 0.20	6.45E-08	6.2
HK-8	25°18'15.4"	39°32'42.7"	Jarad	alkali basalt							10.2
HK-9	25°23'12.2"	39°26'48.6"	Jarad	alkali basalt	2.29	0.01	67.0	0.67			5.5
HK-10	25°23'13.0"	39°23'43.8"	Jarad	alkali basalt	2.33	0.01	58.0	0.93			5.7
HK-17	25°58'12.3"	39°22'35.6"	Jarad	alkali basalt	1.05	0.01	96.0	0.82			8.1
HK-18	25°55'48.5"	39°20'36.4"	Jarad	alkali basalt	1.05	0.01		1.15			8.3
HK-20	25°45'40.9"	39°17'43.4"	Jarad	alkali basalt	1.70	0.01	71.1	0.65			10.7
HK-24	25°34'41.4"	39°19'25.2"	Jarad	alkali basalt	0.390	0.007		0.58			10.4
Kura-2	25°36'58.4"	39°17'09.5"	Jarad	alkali basalt	1.75	0.03	95.6	1.18			
HK-7	25°18'13.2"	39°32'59.0"	Kura	phonolite	8.39	0.02	45.5	0.80			4.7
HK-11	25°19'23.0"	39°16'22.2"	Kura	alkali basalt	6.32	0.02					3.9
HK-12	25°20'04.6"	39°15'13.3"	Kura	alkali basalt					no olivine?		3.9
HK-14	25°24'51.8"	39°10'57.9"	Kura	alkali basalt	5.90	0.02	35.7	1.25			3.2
HK-13	25°20'33.0"	39°13'37.9"	Kura	alkali basalt	6.09	0.02	60.5	1.36	12.02 ± 0.22	2.13E-08	3.3
HK-15	25°28'17.9"	39°12'52.9"	Kura	alkali basalt	6.42	0.02		0.54	12.70 ± 0.22	1.16E-08	3.4
HK-21	25°17'06.9"	39°20'35.2"	Kura	alkali basalt	6.27	0.02	27.8	1.04	12.18 ± 0.22	2.37E-08	3.3
HK-22	25°22'33.8"	39°21'39.3"	Kura	alkali basalt	5.89	0.02		1.42			3.6
HK-23	25°27'47.2"	39°20'57.1"	Kura	alkali basalt	6.06	0.02		1.42			3.8
Kura-1	25°34'49.4"	39°17'21.8"	Kura	alkali basalt	6.00	0.03	41.7	0.66			
Kura-4	25°34'52.5"	39°12'24.0"	Kura	alkali basalt	6.18	0.04	51.2	9.06			
Kura-6	25°26'33.1"	39°17'27.1"	Kura	alkali basalt	6.04	0.02	45.4	0.87			
Ages calculated using monitor FCs sanidine (28.201 Ma, Kuiper et al., 2008) and the total decay constant l = 5.530E-10/yr.											
MSWD is an F-statistic that compares the variance within step ages with the variance about the plateau age.											

Seismic Data Analysis

Calculation of Green functions

The waveform data used to perform the present study was taken from the permanent Broadband stations operated by the Saudi Geological Survey (SGS). All instruments used in the present analysis consist of Nanometrics trillium 120 s velocity sensor and tirnitin digitizers. Figure 10 shows the map of the locations of seismic stations used to process the cross-correlation analysis. We ignored to correct the instrument response because the cross-correlation was applied on the waveforms of matched instrumental responses. As a matter of fact, the cross-correlation removes the common instrumental phase response and amplifies the effect of the instrumental amplitude response. This distortion in amplitude is removed by a whitening step. This is used to diminish the influence of earthquakes and the non-stationary noise sources at the vicinity of the seismometers.

Generally, the cross-correlation calculated between station pairs with a longer time series length yield higher signal to noise ratios (Bensen et al., 2007). In the present analysis, we used the digital waveform data of six months from 1 January to June 2014 as extracted in seed format from the continuous buffer. To increase signal to noise ratio, the extracted traces are processed in 46 half-hour segments starting from 00:30 and ending at 23:30 to avoid possible data loss at the beginning and end of the day due to the start and end time of the original raw data. The half-hour segments are spectrally whitened to produce a flat amplitude spectrum in the 0.05-5 Hz band tapered to zero at 0.02-8 Hz band. The whitened traces are then cross-correlated of matched instrumental responses that eliminated the phase bias of instruments. All 46 half-hour cross-correlations are stacked with their time-reversed cross correlation to create a symmetric day cross correlation.

All available day stacks for a given station pair are stack to retrieve the empirical Green's functions. For this processing, we used and modified some scripts in computer programs in seismology (Herrmann and Ammon, 2004). Empirical Green's functions were obtained for Rayliegh wave along all possible combinations of station pairs. Figure 11 demonstrates a sample example of the cross-correlation Green's function between the vertical component recordings.

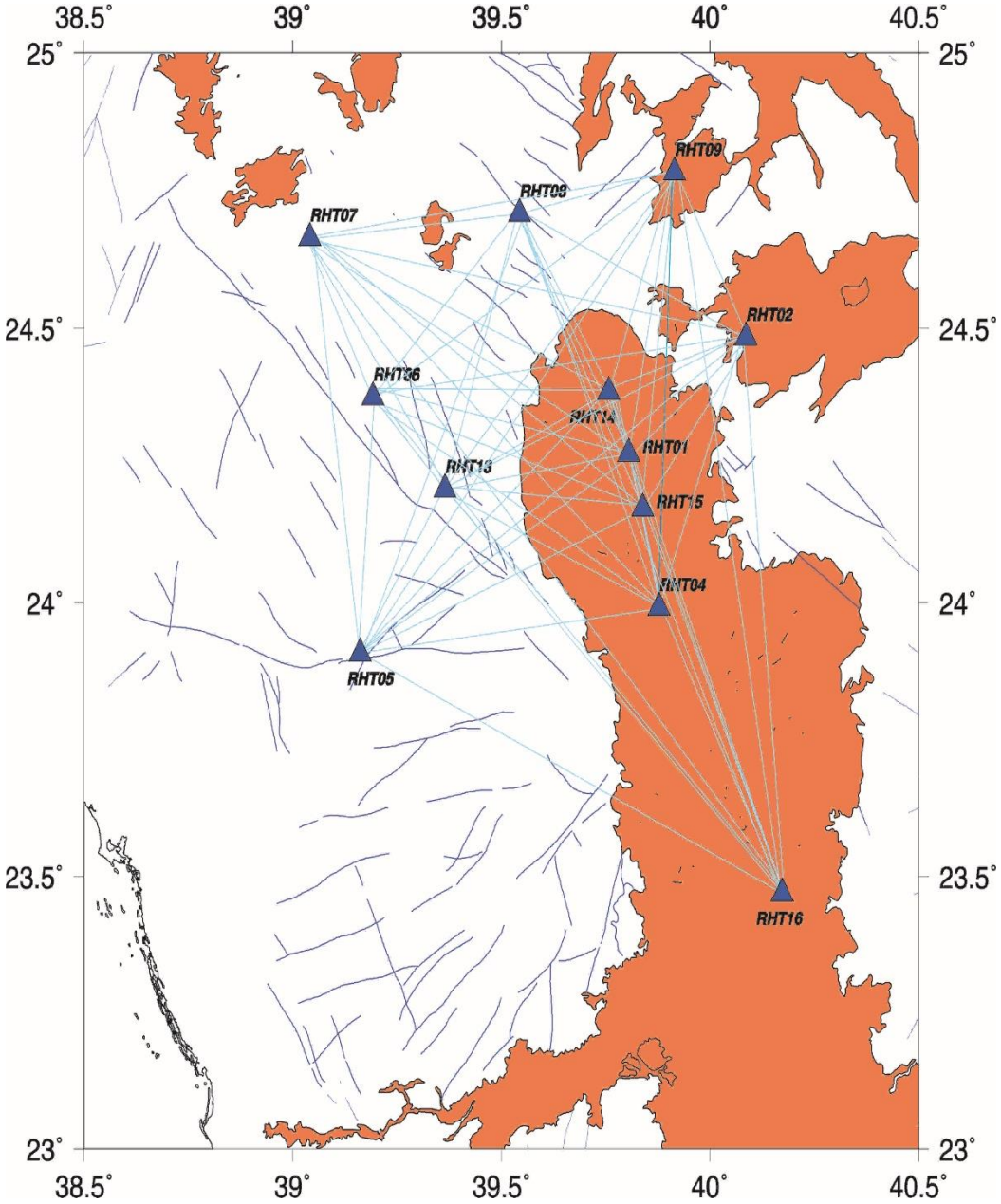

Figure 10. Map shows the location of the broadband seismic stations. The ray-path density between station pairs is also shown for the period of 4 S.

Group velocity measurements

The Rayliegh-wave fundamental mode dispersion curves were measured from each empirical Green's function using a multiple-filter technique (Herrmann, 1978). The group velocity dispersion curves were measured for which station pairs have separated by at least two wavelengths to satisfy the assumption of applying the cross-correlation technique using ambient seismic noise (Brenguier et al., 2007). We picked only the clear dispersion curves and rejected the distortional ones. Figure 9 displays an example of the variation in group velocities versus their corresponded periods as obtained from the multi-filter analysis (MFA) to the vertical components between station pairs. The band pass filtered signal is displayed to the right. The data trend was removed and the seismograms were band-pass filtered with corners at 0.03 and 1 Hz of second order.

The interpretation of contour plots produced by the MFA is often problematic at long periods because of the flattening of the dispersion curves and the decreased signal-to-noise ratio. We were able to measure group velocities of the Rayleigh wave at periods between 1 and 15 s where the main energy is tapered. The maximum number of 138 ray paths was reached at a period of frequency 4 s. Figure 11 shows examples of dispersion measurements along a number of ray paths.

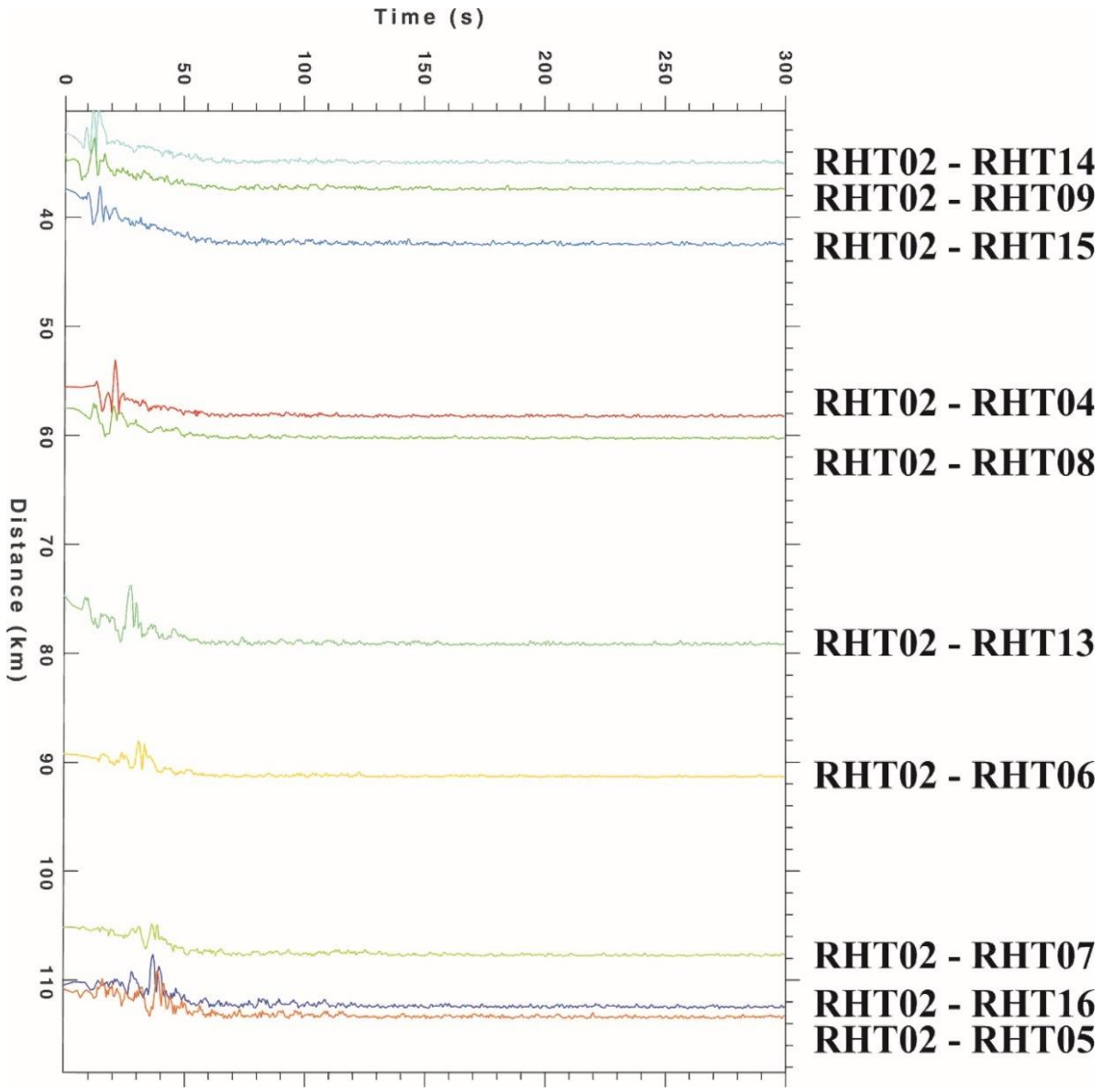

Figure 11. Examples of computed vertical-component interstation cross correlation with respect to the station RHT02.

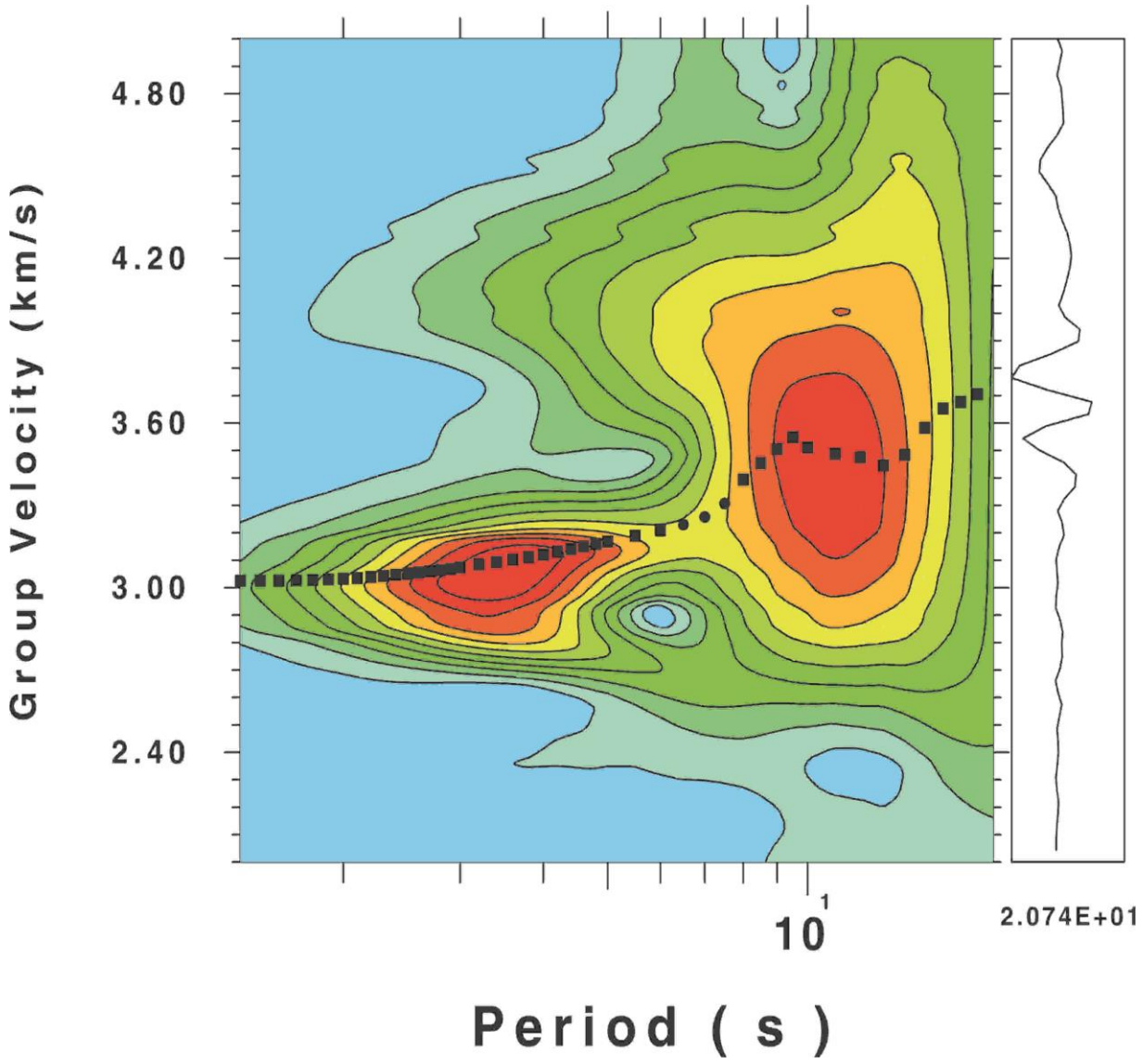

Figure 12 Frequency-time diagram of the fundamental mode of the Rayleigh wave obtained between stations RHT02 and RHT16.

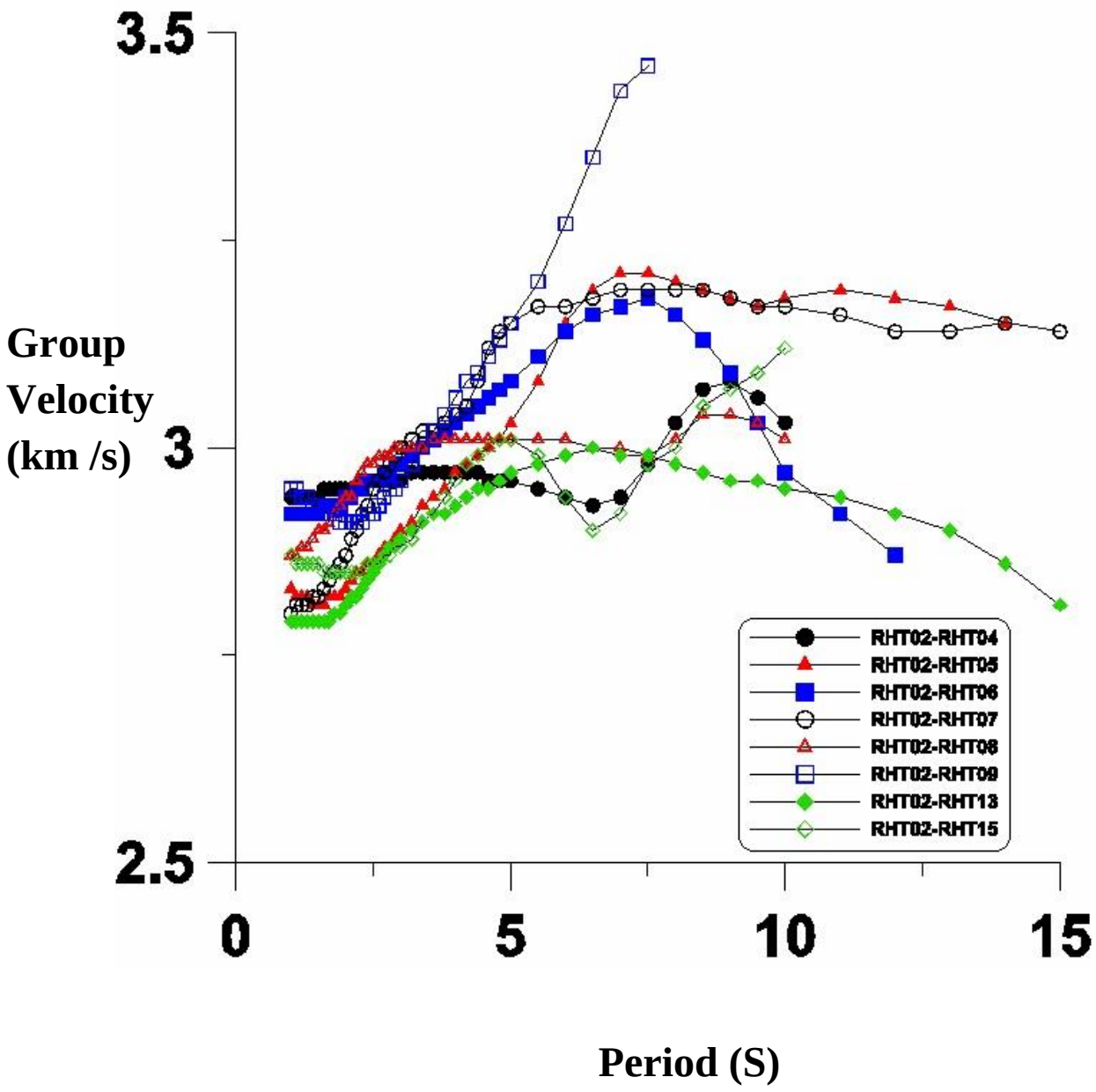

Figure 13. Examples of dispersion curves for station pairs.

Group velocity tomography

Once dispersion curves were measured, we then picked the travel times at different selected period from 1 to 15 s using the group velocities of fundamental modes and the interstaion distance between station pairs. Maps of Rayleigh-wave group velocity tomography were obtained from the non-linear iterative 2-D tomographic technique for the picked travel times (Rawlinson et al., 2008).

During the inversion course, the ray paths between station pairs were simultaneously updated to take into account the influence of the ray lengths in computing theoretical arrival times. This inversion technique uses the Fast Matching Method, which is used in this study to depict group velocity tomography of Raleigh wave in the study area. The FMM is based on a grid Eikonal solution that uses implicit wave front construction and provides stable and robust solutions for wave propagation in highly heterogeneous regions such as tectonic and volcanic environments.

The starting model used in the inversion is a half-space velocity model. The S-wave velocity is the only free parameter in each layer. The inversion scheme searches for the perturbation in the model parameters until the best match of the group velocity is recovered. A discretized grid of 0.2^{o} x 0.2^{o} cells was used to perform the tomographic inversion at each period, which reflected a reasonable resolution and stability of the inversion results. To investigate the geometric resolution of the ray paths representing our observations, a synthetic check board tests were performed. Each test model was assigned a constant velocity perturbed of ±0.5 km/s. Synthetic arrival times for all station pairs were calculated and inverted with the same smoothing and damping parameters used for the observational data. Figure 13 shows

the checkboard resolution test for the same paths as for the observed Rayleigh waves at different periods for the grid size of 0.1^o x 0.1^o cells.

To obtain depth resolution, we inverted a one dimensional velocity model at the nodes of each grid. The dispersion curves were inverted using the SURF96 in computer programs in seismology (Herrmann and Ammon, 2004). The velocity structure fitted to the dispersion curves is displayed in Figure 14 a at a number of grid nodes. Both observed and theoretical dispersion curves corresponding to the obtained velocity model are shown in Figure 14b.

Dispersion curves for each node were constructed by combining the velocity models obtained at at the corners of each grid that smoothed together and placed in the center of each cell falling within the corresponded grid. Figure 15 depicts horizontal slices across the three-dimensional shear wave velocity model at depths of 5, 10, 15, 20, and 25 km.

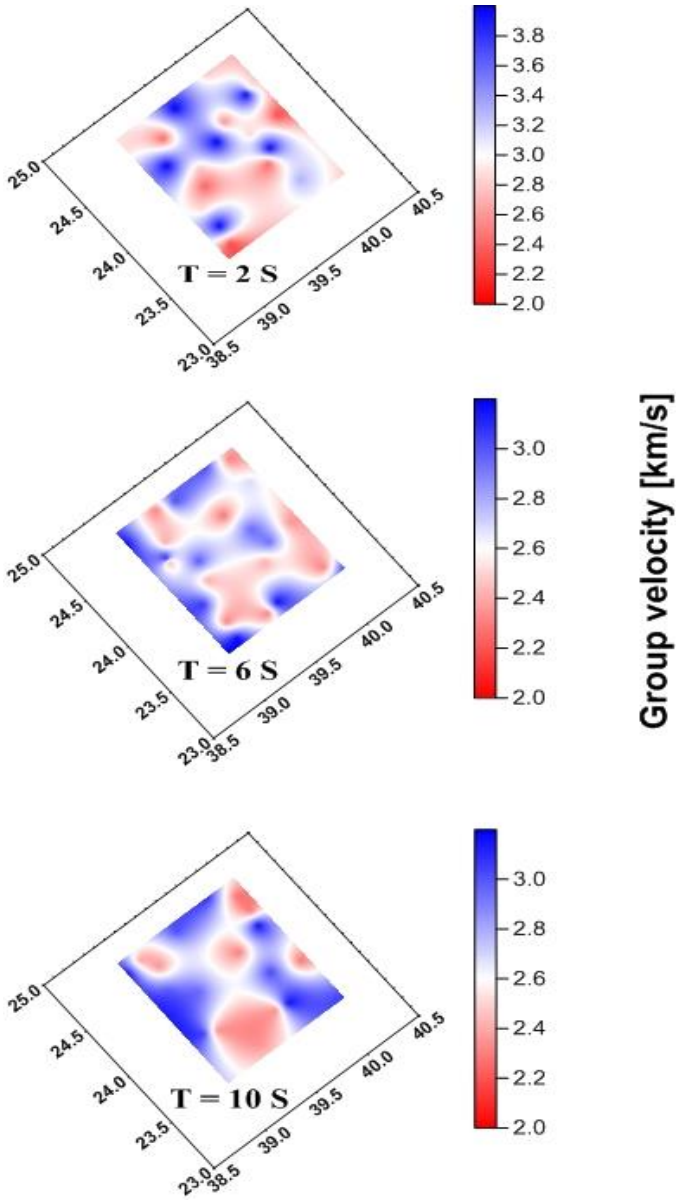

Figure 14. Checkboard resolution analysis for the grid size of 0.1° x 0.1°.

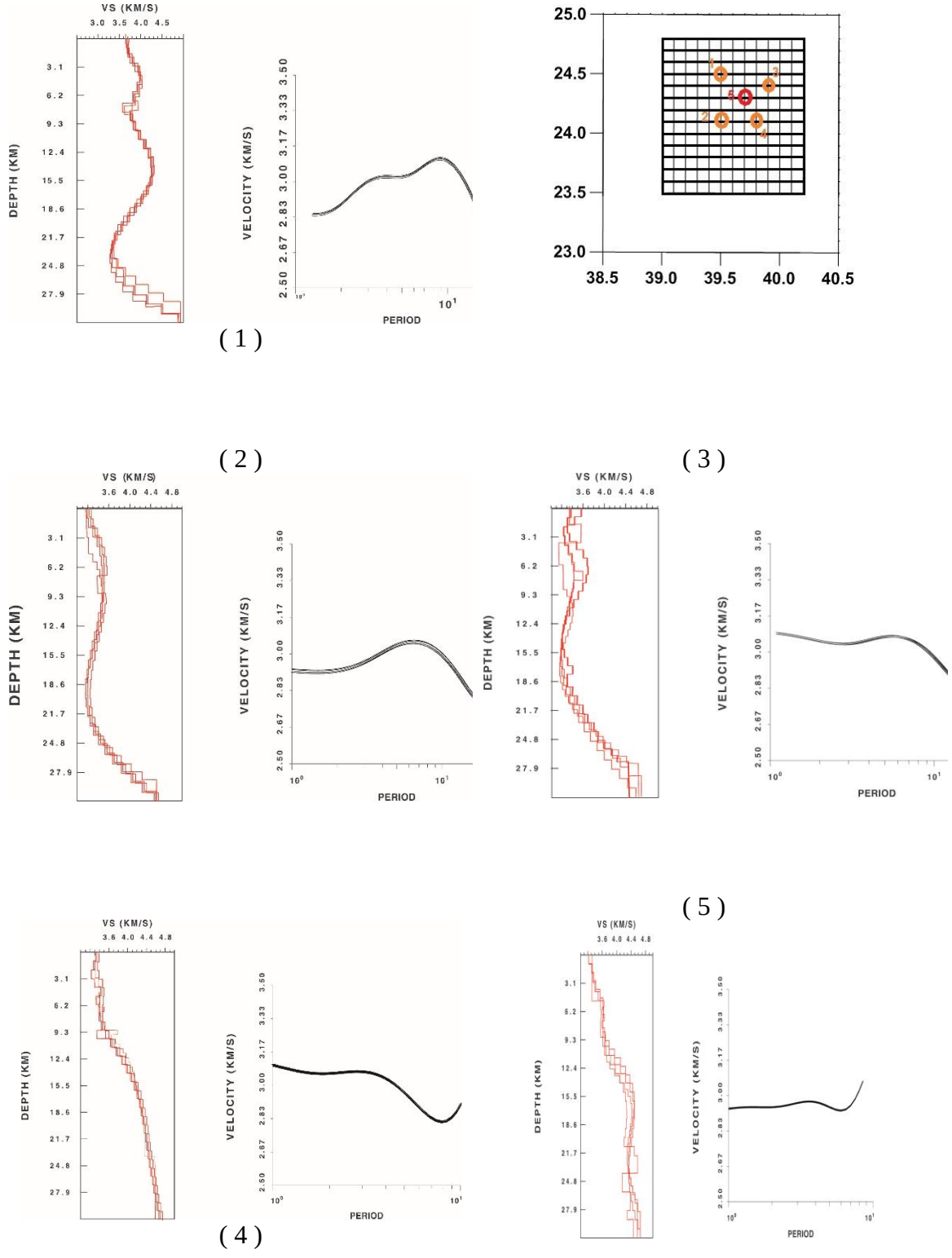

Figure 15. Selected examples for the shear wave velocity versus depth inversion and their locations. One-dimensional velocity models are referred with a number that is written on the location map.

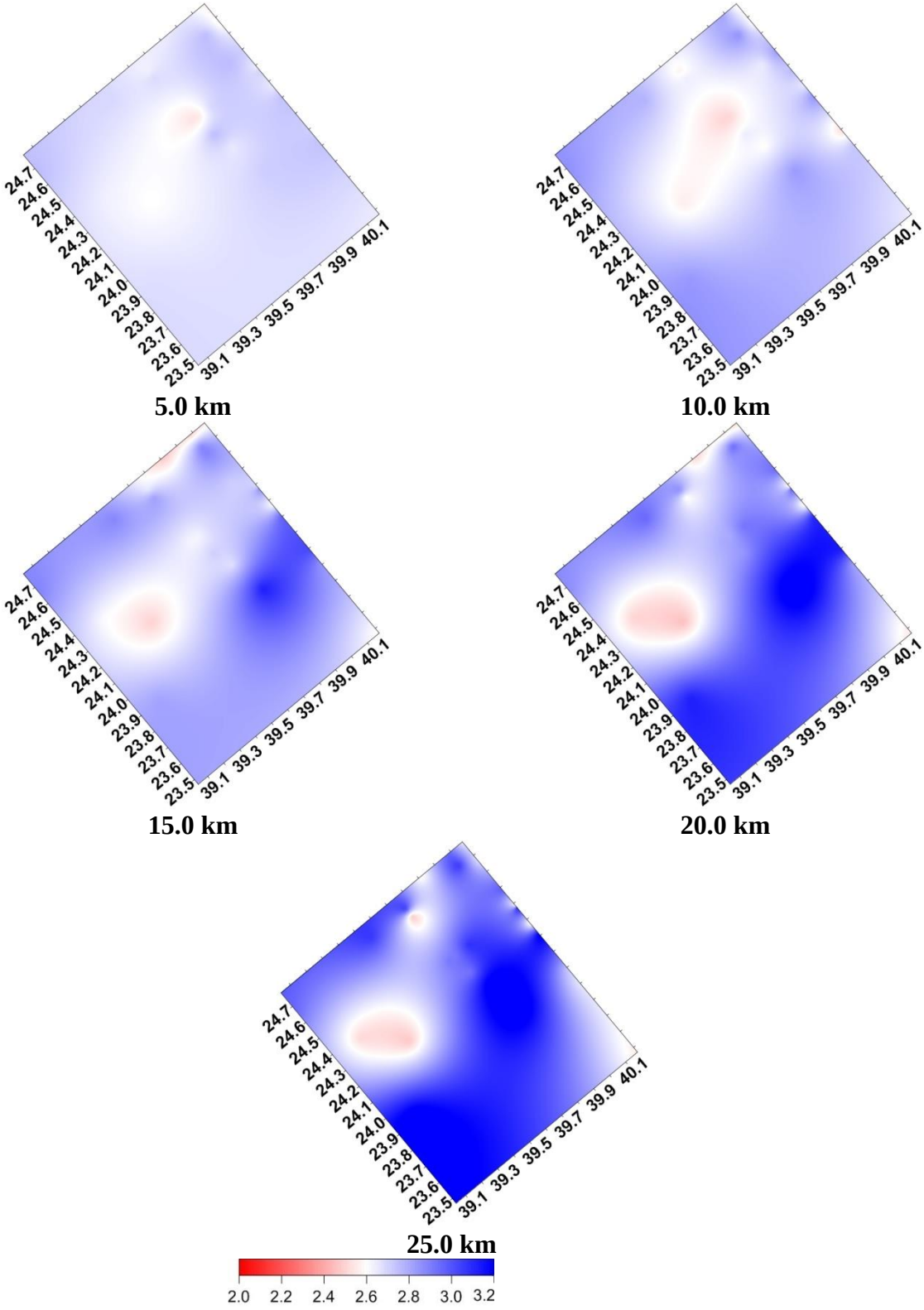

Figure 16. Horizontal slices through the three dimensional shear wave velocity model for the selected depths of 5, 10, 15, 20, and 25 km.

Discussion & Interpretation

Evaluation and Integration of Entire Datasets

The new age determinations and volcanic rock compositions (major, trace and rare earth elements, He-isotopes) now allow us to assemble a temporal picture of development of our studied transect across the harrats province. Our most significant conclusions are the following:

1. Age determinations (^{40}Ar-^{39}Ar incremental heating method). Volcanic activity in the transect area began with eruption of Kura unit alkali basalt magmas as early as 8.4 Ma. A major break in activity occurred between 5.9 and 1.7 Ma, followed by more or less continuous activity up to the present. The Lunayyir harrat has been active 600 ka to the present; the Hutaymah harrat from 850 ka to the present. All centers have exhibited geologically recent activity (i.e., Holocene, younger than 10 ka). However, rocks younger than about 20 ka cannot be precisely dated by the ^{40}Ar-^{39}Ar incremental heating method, and further resolution of age relationships among the youngest eruptions will require other methods, such as ^{14}C. A significant outcome of our dating studies was the recognition of errors in previously reported K-Ar age determinations, due to mantle-derived ("excess") ^{40}Ar contributed by xenolithic material. Hence, activity at Lunayyir and Hutaymah is considerably younger than previously proposed.

2. Major and trace element compositions (X-ray fluorescence and ICP-MS methods). Lava flows and cinder cones in the harrats transect are predominantly of alkali basalt composition, and quite distinct from the tholeiitic basalt compositions of the Red Sea floor and margins (Figure 3). This is a result of differing melting conditions (shallow and extensive under the Red Sea, deeper and less melting under

the Arabian shield), and probably differing mantle source compositions (depleted asthenosphere vs somewhat enriched). Rocks at Lunayyir and Hutaymah fall entirely within the alkali basalt and basanite fields, indicating little modification of magmas rising from the mantle to eruption sites at the surface. At Harrat Khaybar, however, evolved compositions such as trachytes and phonolites occur, which indicate that magmas have accumulated in shallow level crustal chambers, and have fractionated by removal of minerals such as olivine, clinopyroxene and plagioclase. Evidence for the importance of crustal magma chambers at this harrat is also seen in the development of large central volcanoes (i.e., Jabal Qidr, Jabal Abyad). The implication is that much larger volumes of magma have been produced at Harrat Khaybar, compared with Lunayyir and Hutaymah, leading to large-scale replacement of continental crust and lithosphere with young basaltic magmas.

Trace element concentrations and their ratios are very useful in determination of depth and extent of melting of the source region from magmas. For example, the elements Zr and Nb are both partitioned into melt, but Nb more so than Zr at small degrees of melting. Thus, the ratio Zr/Nb is an indicator of extent of melting. In Khaybar lavas, we see that early-erupted flows (8.4-5.9 Ma) have Zr/Nb about 3-4, whereas later erupted flows (1.7-0 Ma) have values of 6-13. We conclude that in spite of greater volumes of lava erupted in the early history of the Khaybar system, individual magmas were derived from relatively small degrees of partial melting of the mantle. With time, individual magmas were derived from greater extents of melting. Other trace elements, such as the rare earth elements (REE), are indicators of depth of melting. The heavy rare earth elements are compatible in the crystal structure of garnet, which is a high pressure mineral stable in the mantle at depths of ~60 km or more. The ratios of light rare earth to heavy rare earth elements (La/Sm vs Dy/Yb,

Figure 17) are used to determine the depth of beginning melting (solidus pressure expressed in giga-pascals, GPa) and depth of last equilibration of melt with mantle residue (lithospheric thickness; 2GPa ~ 60 km depth). From Figure 17 we conclude that Hutaymah and Lunayyir lavas were generated at depths of 60-80 km and small degrees of melting (1-10%), while Khaybar and Rahat lavas were generated under a progressively thinning lithosphere (60-36 km) and increasing extents of melting.

3. He-isotopic compositions (Noble gas mass spectrometry). Isotopic geochemistry is used to identify the composition and history of the source of melting to produce magmas. He-isotopes are particularly useful in distinguishing lithosphere from mantle that has been depleted by previous removal of melts, or from 'primitive' mantle (that has not interacted with lithosphere in melting events). The consensus view holds that the upper mantle underlying the lithosphere (asthenosphere) partially melts (and so is 'depleted') whenever plates separate at spreading ridges or in back-arc basins, and is well-mixed world-wide. It has a He-isotopic composition ($^3He/^4He$ relative to the atmospheric ratio, R_A) of 7-9 R_A. Lithosphere that is derived from melting of the upper mantle also has this small range of isotopic compositions. In contrast, primitive mantle, which lies below the depleted upper mantle and is delivered to the earth's surface by mantle plumes only at hotspots (e.g., Hawaii, Iceland), exhibits He-isotopic compositions >10 R_A. An extensive study of lavas and xenolithic fragments from Hutaymah (Konrad et al., 2015) showed that all volcanic and source materials are derived from depleted asthenosphere and lithosphere. Our new data from Khaybar show that initial lavas (6-8 Ma age) have significantly higher He-isotopic compositions (12-13 R_A), while younger lava compositions are within the range of asthenospheric values. Higher values have also been reported for Harrat Rahat, just to the south of Khaybar, by Murcia et al. (2105).

Evaluation of Competing Geodynamic Models

In this study we have produced new data that allows us to constrain the geodynamic processes that lead to harrat magmatism. The key issues we address in this research concern the ultimate causes of melting, specifically: (i) the role of asthenosphere vs. lithosphere in the production of harrat magmas; (ii) systematic changes in the depth and extent of melting in space and time, and the relation between melting and mantle thermal structure, and (iii) the potential role of mantle plume material in harrat volcanism.

Competing geodynamic models fall into two broad categories: passive and active. For approximately the last 30 million years, the Arabian plate has been separating from the African plate along the Red Sea and Gulf of Aden spreading ridges (Figure 1). New sea floor has been created by upwelling and decompression melting of the upper mantle beneath these sites. Lithospheric extension can affect the margins of these new plate boundaries, producing normal faulting and thinning of the lithosphere. Both processes decrease with distance away from the spreading ridges. Thus, the harrat volcanic provinces could result as a passive response to lithospheric faulting and thinning near the plate edges. We would expect, however, that volcanic activity would be symmetrically distributed on either side of the Red Sea, that intensity of volcanism would decrease away from this plate boundary, and volcanic systems would be structurally controlled by faulting parallel to the Red Sea orientation (i.e., NW-SE) – None of these effects is observed. Instead, harrat volcanic systems are distributed as much as ~500 km inland from the Red Sea on the Arabian plate (but largely absent on the African plate), the largest systems (e.g., Khaybar, Rahat) are situated in the center of the province (not close to the Red Sea), and the main

structural fabric (the Makkah-Madinah-Nafud lineament) is oriented N-S rather than parallel with the Red Sea.

Active geodynamic models (e.g., Camp and Roobol, 1992; Krienitz et al., 2009) involve flow of the upper mantle into the region, either from below or laterally, to provide anomalously hot material for melting, lithospheric thinning by thermal erosion, and uplift due to buoyancy. Vertical flow could be in the form of several small mantle plumes, located beneath the largest volcanic systems (Chang and van der Lee, 2011). Northward lateral flow could occur from the Afar region, a known mantle plume that burst into activity at about 32 Ma (Chang and van der Lee, 2011). Considerable support for these asthenospheric flow models comes from seismic imaging (e.g., Hansen et al., 2006, 2007). Our new results also support active geodynamic models:

1. Age determinations document development of a long-lived volcanic system in the Khaybar region (8.4 Ma to present). Lava compositions indicate deep (60-80 km) melting initially, with progressively shallower melting (to 36 km) with time. This is consistent with smaller degrees of melting early and greater degrees with lithospheric thinning. Such a history is consistent with thermal erosion of the lithosphere

2. He-isotopic compositions of some of the Khaybar and Rahat lavas (with values >10 R_A) indicate involvement of mantle plume material. We cannot distinguish flow from directly beneath these systems from lateral flow north from the Afar region. Further study of volcanic systems to the south of our transect could resolve this question.

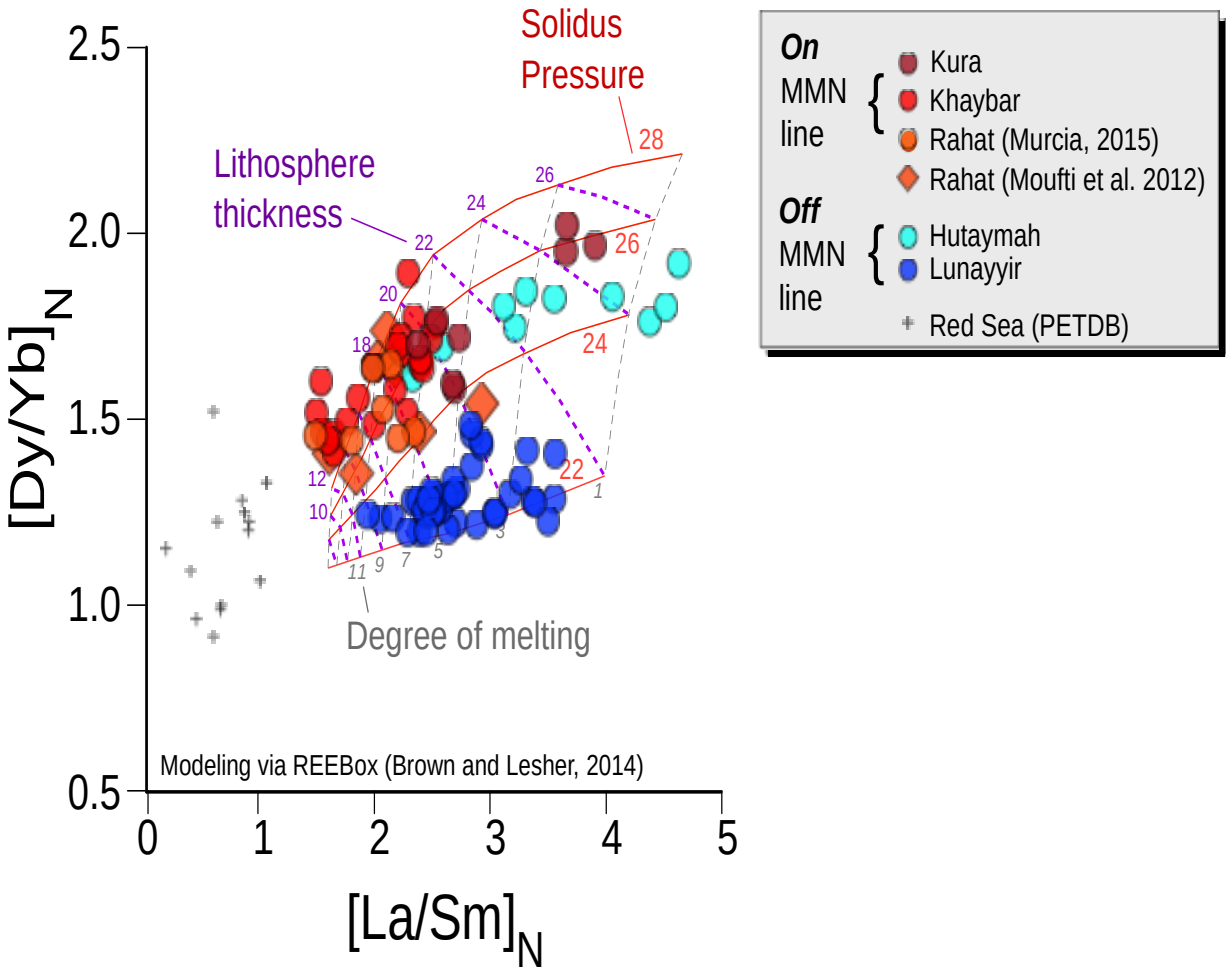

Figure 17. Rare Earth elements (REE) Dy, Yb, La and Sm are used to constrain the depth and degree of melting of the mantle beneath the harrat province. Dy/Yb is the slope of the heavy REE, which are most sensitive to the presence of garnet in the source region – the steeper the deeper. La/Sm is the slope of the light REE, which is more sensitive to degree of melting – inversely correlated. Hutaymah and Lunayyir magmas were generated at depths of 60-80 km (2.2-2.6 GPa) and small degrees of melting (1-10%), while Khaybar and Rahat magmas were generated under a lithosphere of 36-60 km thick (1.2-2.0 GPa). Some of the earliest eruptions (Kura unit) came from deeper (75 km).

Conclusions & Recommendations

Measurements of He-isotopic compositions in harrat Khybar are remarkably homogeneous at 8.2 ± 0.1 R_A (2s, n=3). Major, trace and rare earth element compositions are similar to neighboring (to the south) Harrat Rahat, and indicate that primitive magmas formed from 10-18% partial melting of depleted peridotite at 15-40 km depth. In addition, we see an intriguing trend of increasing degrees of melting at shallowing depths, with time (Zr/Nb and La/Yb trends), which we interpret as evidence for thinning of the lithosphere.

In contrast, magmas at Harrat Lunayyir (100 km east of the Red Sea) formed at 65-80 km depth from 8-12% upper mantle partial melting. Tholeiitic magmas erupted at the Red Sea spreading axis derive from ~ 25% partial melting of upwelling depleted upper mantle, at depths of 0-10 km. This regional variability in mantle melting can be explained by modest lithospheric extension and mantle decompression melting coupled with northward asthenospheric flow from the Afar hot spot (Figure 18). However, a geochemical contribution to harrat volcanism from Afar plume material is so far missing, or very minor.

Lithosphere that is derived from melting of the upper mantle also has this small range of isotopic compositions. In contrast, primitive mantle, which lies below the depleted upper mantle and is delivered to the earth's surface by mantle plumes only at hotspots, exhibits He-isotopic compositions >10 R_A. Lavas and xenolithic fragments from Hutaymah showed that all volcanic and source materials are derived from depleted asthenosphere and lithosphere. Our new data from Khaybar show that initial lavas (6-8 Ma age) have significantly higher He-isotopic

compositions (12-13 R_A), while younger lava compositions are within the range of asthenospheric values. Higher values have also been reported for Harrat Rahat.

Seismic tomographic inversion showed low shear wave velocity in the range of 2.0-3.2 km/s. The study area is clearly resolved with the lowest group velocity toward the west. It is worthy mentioned that the study area is located toward the northeast of the epicenter of the 19th of May 2009 (ML = 5.4) where the area is presumably enriched with magmatic intrusions.

The crust surrounding the fast intrusion is slower than that suggested by broader-scale models for the Arabian Shield. The largest magnitude events occurred early in the swarm, concentrated at shallow depths (~2-8 km) beneath northern Harrat Lunayyir, and these events are associated with the dyke intrusion.

Geologically, these Harrats may host between 150 and 300 °C geothermal systems, hence its importance as a source for possible energy production. The obtained results imply a possibility of existence of magmatic materials of low shear wave velocity beneath Harrat Khaybar as a result of magma upwelling in the region.

Generally speaking, competing geodynamic models fall into two broad categories: passive and active. Our new results also support active geodynamic models. He-isotopic compositions of some of the Khaybar and Rahat lavas (with values >10 R_A) indicate involvement of mantle plume material. We cannot distinguish flow from directly beneath these systems from lateral flow north from the Afar region. Further study of volcanic systems to the south of our transect could resolve this question.

RECOMMENDATIONS FOR FURTHER INVESTIGATIONS

In order to fully understand the detail geophysical, seismological and the geodynamic processes of Arabian Peninsula, this study recommends an extensive research covering:

A. Installation of strong motion accelerographs in various areas of the Arabian Shield to precisely estimate the attenuation characteristics of the region and to improve seismic hazard parameters.

B. Assessment of seismic hazard in seismically active zones by constructing a probabilistic ground-shaking hazard map. This map will provide an estimate of the level of ground shaking at all sites expected from earthquake sources throughout the region (both local and regional). The map integrates the seismicity, attenuation and sit response factors.

C. A comprehensive study of the geotechnical engineering aspects should be done to account for local site effects and soil amplification.

D. A comprehensive study of seismogenic and faulting sources is needed for seismic zonation and microzonation of the Arabian Shield.

E. Geodetic measurements are recommended in order to identify and quantify very recent neotectonic activity and thus, provide prediction of specific future event and crustal deformation. Geodetic techniques range from ground technique using strain meters and laser-ranging devices to space technique using very-long-baseline radio interferometry (VLBI) and the global positioning system (GPS).

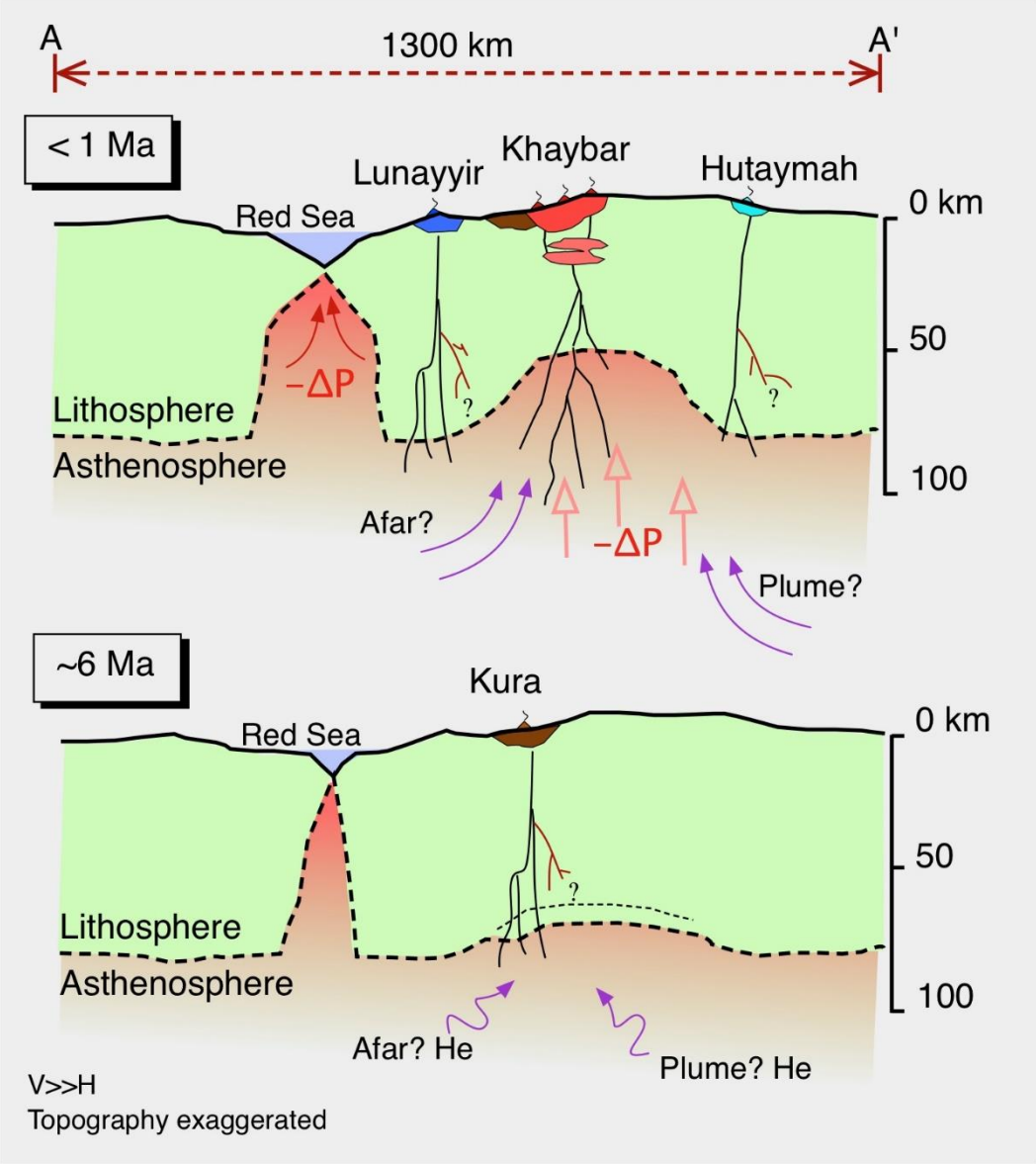

Figure 18. Cartoon cross-section going from the Red Sea to Harrat Hutaymah for two time frames, (<1 Ma and ~6 Ma). The scale is schematic to show features. The boundary layer below the base of the lithosphere contains convective stirring of enriched, delaminated lithosphere with asthenosphere beneath the Makkah-Madinah-Nafud (MMN) lineament and eastward transport in an enriched sub-lithosphere layer to the lithosphere-asthenosphere boundary (LAB) beneath Hutaymah. Geochemical data support geophysical imaging of the LAB, which shows greater thinning under the MMN-line compared with marginal harrats such as Lunayyir and Hutaymah.

References

Bensen, G.D., Ritzwoller, M.H., Barmin, M.P., Levshin, A.L., Lin, F., Moschetti, M.P., Shapiro, N.M. and Yang, Y., 2007. Processing seismic ambient noise data to obtain reliable broad-band surface wave dispersion measurements, Geophys. J. Int., 169, 1239–1260.

Brenguier F, Shapiro N.M, Campillo M, 2007. 2 - 3-D surface wave tomography of the Piton de la Fournaise volcano using seismic noise. Geophysical Research Letters V. 34 Issue: 2.

Camp, V.E., Hooper,P.R., Roobol, M.J. and White, D.L., 1987. The Madinah eruption, Saudi Arabia: Magma mixing and simultaneous extrusion of three basaltic chemical types: Bulletin Volcanology, v. 49, p.489-508.

Camp, V.E., Roobol, M.J. and Hooper, P.R., 1991a.The Arabian continental alkali basalt province: Part II. Evolution of Harrats Khaybar, Ithnayn, and Kura, Kingdom of Saudi Arabia: Bulletin, Geological Society of America, v. 103, p.363-391.

Camp, V.E., Roobol, M.J., and Hooper, P.R., 1991b. The Arabian continental alkali basalt province: Part III. Evolution of Harrat Kishb, Kingdom of Saudi Arabia: Bulletin, Geological Society of America, v. 104, p. 379-396.

Camp, V.E. and Roobol, M.J., 1992. Upwelling asthenosphere beneath western Arabia and its regional implications. J. Geophys. Res. 90, 15,255–15,271.

Chang, S. J. and van der Lee, S., 2011. Mantle plumes and associated flow beneath Arabia and East Africa., Earth Planet. Sci. Lett., 302: 448-454.

Duncan, R. A. and Al-Amri, A. M., 2013. Timing and composition of volcanic activity at Harrat Lunayyir, Western Saudi Arabia. J. volcano. Geotherm. Res., 260: 103 -116.

Duncan, R.A., Kent, A.J.R., Thornber, C.R., Schlieder, T.D., and Al-Amri, A.M. 2016. Timing and composition of continental volcanism at Harrat Hutaymah, western Saudi Arabia, J. Volc. Geoth. Res, 313, 1-14.

Fram, M.S. and Lesher, C.E., 1993. Geochemical constraints on mantle melting during creation of the North Atlantic basin. Nature, 363: 712-715.

Hansen, S., Thurber, C., Mandernach, M., Haslinger, F., and Doran, C., 2004. Seismic velocity and attenuation structure of the East Rift Zone and South Flank of Kilauea Volcano, Hawaii. Bull. Seism. Soc. Am., 94, 1430-1440.

Hansen, S., Schwartz, S., Al-Amri, A. and Rodgers, A., 2006. Combined plate motion and density driven flow in the asthenosphere beneath Saudi Arabia: evidence from shear- wave splitting and seismic anisotropy. Geology, V. 34, no. 10, p. 869 – 872.

Hansen, S., Rodgers, A., Schwartz, S., and Al-Amri, A., 2007. Imaging ruptured lithosphere beneath the Red Sea and Arabian Peninsula. Earth and Planet. Sci. Letters, 259: 256 – 265.

Hempton, M.R., 1987. Constraints on Arabian plate motion and extensional history of the Red Sea. Tectonics 6: 687-705.

Herrmann, R. B., 1978. Computer programs in earthquake seismology Vol.1: General programs, Department of Earth and Atmospheric Sciences, St. Louis University.

Herrmann, R.B. and Ammon, C.J. 2004. Surface Waves, Receiver Functions and Crustal Structure, Computer Programs in Seismology, Version 3.30. Saint Louis University, Saint Louis

Johnson, P.R. 2000. Proterozoic geology of Saudi Arabia: Current concepts and issues. Contribution to a workshop on the geology of the Arabian Peninsula, 6th meeting of the Saudi Society for Earth Science, King Abdulaziz City for Science and Technology, Riyadh, Saudi Arabia.

Kent A.J.R, Baker J.A., Wiedenbeck M., 2002. Contamination and melt aggregation processes in continental flood basalts: constraints from melt inclusions in Oligocene basalts from Yemen. Earth Planet Sc. Lett 202: 577-594.

Kent, A.J.R., 2008. Melt inclusions in basaltic and associated volcanic rocks. Rev. Mineral. Geochem., 69,173-231.

Konrad, K., Graham, D.W., Thornber, C.R., Duncan, R.A., Kent, A.J.R., and Al-Amri, A. 2016. Asthenosphere-Lithosphere Interactions in Western Saudi Arabia: Inferences from 3He/4He in Xenoliths and Lava Flows from Harrat Hutaymah, Lithos, 248–251, 339–352.

Krienitz, M.S., Haase, K.M., Mezger, K., van den Bogaard, P., Thiemann, V., Shaikh-Mashail, M.A., 2009. Tectonic events, continental intraplate volcanism, and mantle plume activity in northern Arabia: constraints from geochemistry and Ar–Ar dating of Syrian lavas. Geochem. Geophys. Geosyst. 10. http://dx.doi.org/10.1029/2008GC002254.

McDougall, I. and Harrison, T.M., 1988. Geochronology and Thermochronology by the 40Ar/39Ar Method. Oxford University Press, New York, 212pp.

McKenzie D. and M .J. Bickle, 1988. The volume and composition of melt generated by extension of the lithosphere. J. Petrol., 29: 625-679.

Moufti, M.R.H. and Hashad, M.H. 2005. Volcanic hazards assessment of Saudi Arabian Harrats: geochemical and isotopic studies of selected areas of active Makkah- Madinah-Nafud (MMN) volcanic rocks. Final Project Report (LGP-5-27), King Abdlaziz City for Science and Technology, Riyadh, Saudi Arabia.

Murcia, H., Nemeth, K., El-Masry, N.N., Lindsay, J.M., Moufti, M.R., 2015. The Al-Du'aythah volcanic cones, Al-Madinah City: implications for volcanic hazards in northern Harrat Rahat, Kingdom of Saudi Arabia, Bulletin of Volcanology, 77(6), No. 54.

Pallister, J. S.; Wendy. A.; McCausland, S. Jónsson; Z. Lu; H..Zahran;S.El Hadidy; A. Aburukbah ; I.Stewart; P. Lundgren; R. White and M.R. . Moufti 2010. Broad accommodation of rift-related extension recorded by dyke intrusion in Saudi Arabia. Nature Geoscience, DOI: 10.1038/NGE0966.

Pesicek, J.D., Thurber, C.H., Zhang, H., DeShon, H.R., Engdahl, E.R., and Widiyantoro, S., 2010. Teleseismic double-difference relocation of earthquakes along the Sumatra-Andaman subduction zone using a three-dimensional model, J. Geophys. Res., 115, doi: 10.1029/2010JB007443, 2010.

Rawlinson, N, Sambridge, M and Saygin, E., 2008. A dynamic objective function technique for generating multiple solution models in seismic tomography, Geophysical Journal International, vol. 174, pp. 295-308.

Roobol, M.J. and Camp, V.E., 1991a. Geologic Map of the Cenozoic Lava Field of Harrat Khaybar, Kingdom of Saudi Arabia: Saudi Arabian Directorate General of Mineral Resources Geoscience Map GM-131, scale 1:250,000 with text 37p.

Roobol, M.J. and Camp, V.E., 1991b. Geologic map of the Cenozoic Lava Field of Harrat Kishb, Kingdom of Saudi Arabia: Saudi Arabian Directorate General of Mineral Resources Geoscience Map GM-132, scale 1:250,000 with text 34p.

Sato, H., Sacks, I.S., Murase, T., Muncill, G. and Fukuyama, H. 1989. Qp-melting temperature relation in peridoite at high pressure and temperature: attenuation mechanism and implications for the mechanical properties of the upper mantle. Journal of Geophysical Research 94: doi: 10.1029/89JB00738. issn: 0148-0227.

Shapiro, N.M, M. Campillo, L. Stehly, and M.H. Ritzwoller, 2005. High-Resolution surface wave tomography from ambient seismic noise, Science, 307, 1615-1618.

Stoeser, D.B. and Camp, V.E. 1985. Pan-African microplate accretion of the Arabian Shield, Bull. Geol. Soc. Amer. 6: 817-826.

Thornber, C. R., 1992. The petrology, geochemistry and origin of ultramafic inclusions and mafic alkaline volcanic from Harrat Hutaymah, Saudi Arabia, University of Colorado.

Thornber, C., 1994. Ultramafic inclusions from Harrat Hutaymah: A record of mantle magmatism beneath north central Arabia. Proceedings of the International Kimberlite Conference, p. 434.

Thurber, C., 1983. Earthquake locations and three-dimensional crustal structure in the Coyote Lake area, central California, J. Geophys. Res., 88, 8226-8236.

Thurber, C., and Eberhart-Phillips, D., 1990. Local earthquake tomography with flexible gridding, Comp. Geosci., 25, 809-818.

Zhang, H., and Thurber, C., 2003. Double-difference tomography: The method and its application to the Hayward Fault, California, Bull. Seis. Soc. Am., 93, 1875-1889.

GLOSSARY

المصطلحات اللاتينية وترجمتها الى االعربية

Arabian Plate	الصفيحه العربيه
Arabian Platform	الرصيف العربي
Arabian Shield	الدرع العربي
Asthenosphere	الغلاف الوهن
Azimuth	الإتجاه الزاوي
Broadband Stations	محطات واسعة المدى
Correlation Coefficient	معامل المضاهاه
Crustal Structure	التركيب القشري
Crustal Thickness	السمك القشري
Harrat Lunayyir	حرة لونيير
Delay Time	زمن التأخير
Epicenter	المركز السطحي للزلزال
Focal Mechanism Solutions	حلول ميكانيكية البؤرة
Fast Polarization	الإستقطاب السريع
Focal Depth	العمق البؤري
Group Velocities	السرع الجماعية
International Association of Seismology & Physics of the Earth (Iasp91)	نموذج حساب معدل السرعه
Frequency	التردد
Aeromagnetics	المغناطيسية الجوية
Magma	صهارة
Lithosphere	الغلاف الصخري
Chronology	العمر الجيولوجي
Broadband seismic station	محطة رصد ذات فتره دوريه واسعة المدى
Longitude (E)	خط الطول
Lower Crust	القشره السفلي
Magnitude	القدر الزلزالي

Mantle	الوشاح (لحاء)
Miocene	فترة الميوسين
Moho Discontinuity	إنقطاع موهو
Monthly Listing	النشرة الزلزاليه الشهريه
Spreading Centers	مراكز التمدد
Tertiary	العصر الثلاثي
Origin Time	زمن حدوث الزلزال عند البؤره
Preliminary Determination of Epicenters (PDE)	التحديد المبدئي لمراكز الزلازل
Plate Tectonics	حركة الصفائح
Polar Projection	إسقاط قطبي
Primary Wave Velocity (Vp)	سرعة الموجات الطوليه
Quaternary	العصر الرابع
Receiver Function	دالة المستقبل
Response Curve	منحنى الإستجابه
Review Events Bulletin (REB)	نشرة الأحداث المراجعه
Rock Density	الكثافه الصخريه
SANDSN	الشبكه السعودية الوطنيه الرقمية للزلازل
Seismic Analysis Code (SAC)	كود التحليل الزلزالي
Seismic Attenuation	التعتيم الزلزالي
Seismic Hazards	خطر زلزالي
Seismic Noise	الضوضاء السيزميه
Seismic Tomography	زلزالية ثلاثية الأبعاد
Seismic Waves	الموجات الزلزاليه
Seismogram	سجل زلزالي
Shear Wave Velocity (Vs)	سرعة موجات القص
Shear Wave Splitting	فصل موجات القص
Spectral Amplitude	السعة الطيفيه
Spectral Analysis	التحليل الطيفي
Surface Wave dispersion	تشتت الموجة السطحي
Surficial Sediments	رواسب سطحيه
Synthetic Waveform	الشكل الموجي المركب
Take-off Angle	زاوية خروج الشعاع عند بؤرة الزلزال
Teleseismic Earthquakes	الزلازل البعيده
Tertiary	العصر الثالث

Theoretical Spectral Rations	**النسب الطيفيه النظريه**
Thickness	**السماكه**
Transition Zone	**منطقة إنتقاليه**
Travel Times	**أزمنة المسار**
Upper Crust	**القشره العلويه**
Wave Propagation	**الإنتشار الموجي**
Waveform Modeling	**نمذجة الشكل الموجي**